

Resurrecting the coherent state variational algorithm for large N gauge theories

Laurence G. Yaffe*

Department of Physics, University of Washington, Seattle, Washington 98195–1560

The feasibility of studying, numerically, properties of infinite volume QCD-like theories in the large N limit using coherent state variational methods is reassessed. An entirely new implementation of this approach is described, applicable to $SU(N)$ lattice gauge theories, with or without fundamental representation fermions, on cubic lattices of up to four dimensions. In addition to various test cases, initial results are presented for Hamiltonian Yang-Mills theory on an infinite two-dimensional spatial lattice.

CONTENTS

I. Introduction	2
II. Variational Strategy	5
A. State representation	5
B. Variational parameters	9
C. Coherent state variational algorithm	13
D. Why bother?	14
III. The program “Gordion”	15
IV. Results	17
A. Euclidean one-plaquette model	18
B. Hamiltonian one-plaquette model	21
C. 2D Euclidean Yang-Mills	25
D. 2+1D Hamiltonian Yang-Mills	30
V. Observable approximation	33
VI. Discussion	37
VII. Conclusion	41
Acknowledgments	43
References	44

* yaffe@phys.washington.edu

I. INTRODUCTION

For more than forty years, it has been understood that the large N limit of $SU(N)$ (or $U(N)$) gauge theories is a type of classical limit [1]. Suitably defined coherent states provide an overcomplete basis for the gauge-invariant Hilbert space. Off-diagonal coherent state overlaps, as well as off-diagonal coherent state matrix elements of “reasonable” operators,¹ vanish exponentially as the gauge group rank $N \rightarrow \infty$. As a result, one may show that the dynamics of the quantum field theory, in the large N limit, is reproduced by classical dynamics on a phase space essentially isomorphic to the space of coherent states, with a classical Hamiltonian given by the large N limit of the coherent state expectation value of the quantum Hamiltonian (rescaled by N^{-2}). This structure precisely parallels the usual $\hbar \rightarrow 0$ limit of point particle quantum mechanics, with $1/N^2$ playing the role of \hbar . For $SU(N)$ gauge theories containing fundamental representation fermions there is a nested structure to the large N limit, with the large N coherent states of the pure Yang-Mills theory leading to the gauge sector $N = \infty$ classical dynamics, while coherent states of the fermionic degrees of freedom (generated by exponentials of fermion bilinears) lead to an analogous phase space structure and classical dynamics which reproduce the subleading $O(N)$ quantum dynamics of the full theory [2, 3].²

The classical nature of the large N limit implies that “solving” the quantum field theory — meaning accurate computation of ground state and physically relevant low energy properties — reduces, when $N \rightarrow \infty$, to a *classical* minimization problem: finding the minimum of the classical Hamiltonian which reproduces the large N quantum dynamics. In semiclassical point particle quantum mechanics, one expands around the minimum of the classical potential to determine quantum level spacings and anharmonic corrections. Similarly, expanding to quadratic order about the minimum of the large N classical Hamiltonian enables one to compute the frequencies of small oscillation normal modes which, in an $SU(N)$ or QCD-like gauge theory, amounts to determining the low-lying glueball or meson mass spectrum. Cubic terms in the Taylor expansion about the minimum determine the leading large- N behavior of two particle decay amplitudes of mesons or glueballs, while quartic terms determine the leading behavior of two-to-two particle meson or glueball scattering amplitudes.³

The above summary applies directly to lattice regulated gauge theories in a Hamiltonian formulation (i.e., spatial lattice with continuous time). A parallel formulation is applicable to Euclidean gauge theories on a space-time lattice, where the natural language is that of statistical mechanics. Instead of minimizing the expectation value of a quantum Hamiltonian, the goal is to minimize the free energy, viewed as a functional of an arbitrary statistical

¹ Including single trace operators of bounded length, or finite order products of such operators.

² This assumes that the number of fermion flavors is held fixed as $N \rightarrow \infty$.

³ Baryons are solitons in the large N limit [4], with masses scaling as $O(N)$. Computation of large N baryonic properties will not be considered in this paper.

density matrix ρ ,⁴

$$F[\rho] \equiv A[\rho] - S[\rho], \quad (1.1)$$

where the energy (or action) $A[\rho]$ is a linear functional of the density matrix, while the entropy is given by the von Neumann definition,

$$S[\rho] \equiv -\text{tr}(\rho \ln \rho). \quad (1.2)$$

The Boltzmann distribution, $\rho_B \equiv Z^{-1} e^{-A}$, minimizes the free energy (1.1) but, in a non-trivial gauge theory, computing properties of this ensemble is very challenging. As in the Hamiltonian approach, one may define a manifold of “coherent state” statistical ensembles which provide an overcomplete basis, meaning that any statistical density matrix may be expressed as a positively weighted mixture of coherent state density matrices.⁵ For large N , the entropy and free energy of a coherent state density matrix are $O(N^2)$, while the entropy of mixing in a linear combination of such coherent states remains $O(1)$. As $N \rightarrow \infty$, each coherent state density matrix acts like an extremal thermodynamic ensemble in which “reasonable” observables satisfy large N factorization. The coherent state ensemble of minimal free energy is indistinguishable, via measurements of any such reasonable operator, from the exact Boltzmann ensemble. So solving the Euclidean theory in the large N limit reduces to the minimization of the free energy of individual coherent state ensembles, followed by computing physically relevant properties of that minimizing coherent state ensemble.

This coherent state approach for Euclidean theories is, of course, of practical interest only if minimizing the coherent state free energy and computing physically relevant properties is less demanding than performing the stochastic simulations needed to accurately estimate physically interesting properties of the Boltzmann ensemble. The key point is that the coherent state formulation allows one to work directly at $N = \infty$, exploit large N factorization, and entirely avoid both finite volume effects and statistical sampling variance.

The outline of this paper is as follows. Possible variational strategies for both Hamiltonian and Euclidean formulations are discussed in Section II, emphasizing the choices leading to the specific form of the coherent state variational algorithm first presented in Ref. [3]. Section III then briefly describes the recent (re)implementation of this approach in the form of a unified program named *Gordion*. Section IV presents results from one-plaquette model test cases as well as for both 2D Euclidean and 2+1 dimensional Hamiltonian theories on an infinite two-dimensional cubic lattice, using the simple observable truncation scheme described below. The following section V presents results from an initial effort to reduce truncation errors by using a loop-factorization based approximation for expectation values of non-retained

⁴ The factor of temperature which would conventionally multiply the entropy in the free energy expression (1.1) is omitted. One may view this as a choice of units, or equivalently regard the energy A and free energy F used here as $\beta \equiv 1/T$ times the conventional energy and free energy.

⁵ In the gauge sector of a D -dimensional Euclidean theory, these coherent state density matrices are just the absolute squares of coherent state wavefunctionals for a $D+1$ dimensional Hamiltonian theory.

observables. Features, lessons and implications of these various results are discussed in Section VI, while a final section VII offers concluding discussion and remarks.

All results presented in this paper are limited to pure Yang-Mills theories using the simplest Wilson action [5] or Kogut-Susskind Hamiltonian [6]. (A subsequent publication will examine mesonic properties in QCD-like theories with fermions.) All computations presented in this work were performed on a desktop computer,⁶ not on any large cluster or supercomputer. So the presented results should not be regarded as fully exploring the potential of this approach.

There are, of course, other possible approaches for studying large- N gauge theories. Highly developed numerical simulation methods for Euclidean lattice gauge theories, involving Monte-Carlo sampling of gauge field configurations, have been applied to $SU(N)$ Yang-Mills theories in three and four dimensions, for values of N ranging from 2 up to 12 (4D) or 16 (3D) [7–12]. These works have studied the glueball spectrum, k -string tensions, and deconfinement temperatures, with a notable finding of remarkably weak dependence of these physical quantities on N .

There has also been interesting recent work applying so-called “bootstrap” methods [13, 14] to the $N = \infty$ loop equations of Euclidean lattice Yang-Mills theories [15]. This approach combines (subsets of) the lattice loop equations with positivity constraints to derive rigorous inequalities on the range of possible expectation values of selected sets of Wilson loops. Related work has applied similar ideas to finite N Yang-Mills theory [16, 17], as well as various matrix models [18–20].

The direct applicability of the coherent state approach to Hamiltonian lattice gauge theories is one major contrast to these alternative approaches based on Euclidean lattice formulations. The Hamiltonian formulation allows far more direct access to the spectrum of glueballs or mesons, without having to extract masses from the long-distance fall-off of correlation functions. Although not yet fully realized, of even greater significance is the potential to obtain decay widths and two-particle scattering amplitudes from cubic and quartic terms in the Taylor expansion of the large N classical Hamiltonian about its minimum. While there has been significant recent progress in the development of methods to extract mesonic scattering amplitudes from Euclidean lattice simulations [21, 22], this remains a exceptionally difficult endeavor.

Finally, although not yet applicable to non-trivial Yang-Mills theories, there are also interesting recent efforts applying Hamiltonian truncation schemes to model field theories [23]. To date, this approach is very far from reaching the goal of accurate calculations in non-Abelian gauge theories in two or more space dimensions. While the computational challenge involved in applying the coherent state variational method to large N Yang-Mills theories in 2+1 or 3+1 dimensions is very substantial, it seems clear that this classical minimization problem must nevertheless be far more tractable than any direct attack on finite N Yang-Mills theory via Hamiltonian truncation capable of yielding physically interesting results.

⁶ A 2022 Apple Mac Studio with 20-core M1 Ultra cpu, 128 Gb of memory, and 2 Tb of solid state disk.

II. VARIATIONAL STRATEGY

A. State representation

Designing any variational minimization begins with a choice of coordinates, or more generally a choice for how to represent information characterizing properties of individual states in the minimization domain. For large- N lattice Yang-Mills theories, the conceptually simplest, most natural answer is the set of Wilson loop expectation values for all closed paths,

$$\left\{ W_\Gamma \equiv \lim_{N \rightarrow \infty} N^{-1} \langle \text{tr } U_\Gamma \rangle \right\}. \quad (2.1)$$

Here Γ denotes an arbitrary closed path on the lattice, with U_Γ the ordered product of link matrices (or holonomy) around the path Γ .

In Hamiltonian lattice Yang-Mills theory, the loop traces $\{\text{tr } U_\Gamma\}$ are all commuting operators defined at equal time on the spatial lattice. The Wilson loop expectation values (2.1) may be viewed as coordinates on the large- N classical configuration space, i.e., the time-reversal invariant subspace of the large- N phase space.⁷ The associated classical momenta are time-derivatives of these coordinates, which amount to expectations of Wilson loop operators with one electric field insertion,

$$\left\{ W_{\ell, \Gamma} \equiv \lim_{N \rightarrow \infty} N^{-1} \langle \text{tr } E_\ell U_\Gamma \rangle \right\}. \quad (2.2)$$

Here, ℓ labels links on the lattice, E_ℓ is the $U(N)$ electric field operator on link ℓ , and the path Γ starts with link ℓ or ends with the conjugate link $\bar{\ell}$.⁸

In theories with fundamental representation fermions, the set of all fermion bilinear expectation values,

$$\left\{ G_{\Gamma_{xy}} \equiv \lim_{N \rightarrow \infty} \langle \bar{\psi}_x U_{\Gamma_{xy}} \psi_y \rangle \right\}, \quad (2.4)$$

can serve as coordinates on the fermionic large- N phase space. Here x, y label lattice sites, Γ_{xy} is some lattice path from site x to site y , and the fermion fields $\{\bar{\psi}_x, \psi_y\}$ satisfy conventional anticommutation relations. These fermion bilinear expectation values may also be partitioned into time-reversal even “coordinates” and time-reversal odd “momenta” on the fermionic large- N phase space.

⁷ Throughout this work, all theories under consideration possess both time reversal and charge conjugation symmetry.

⁸ The difference between $U(N)$ and $SU(N)$ gauge theories is subleading in the large- N limit, and is irrelevant to this discussion. The $U(N)$ electric field operators satisfy the lattice gauge theory commutation relations,

$$[(E_\ell)_{ij}, (U_{\ell'})_{kl}] = \frac{1}{N} \delta_{\ell\ell'} \delta_{kj} (U_\ell)_{il}, \quad [(E_\ell)_{ij}, (E_{\ell'})_{kl}] = \frac{1}{N} \delta_{\ell\ell'} (\delta_{kj} (E_\ell)_{il} - \delta_{il} (U_\ell)_{kj}), \quad (2.3)$$

with i, j, k, l denoting $U(N)$ gauge indices.

These sets of Wilson loop and fermion bilinear expectations, plus (in Hamiltonian theories) Wilson loop time derivative expectations, encode the information in any large- N coherent state. All such coherent states satisfy large- N factorization, with different coherent states distinguished by differing values in their sets of expectation values.

On a translationally invariant lattice (without spontaneous breaking of translation symmetry, which is assumed throughout), one may identify expectation values of operators which merely differ by a lattice translation. Likewise for observables related by other lattice symmetries (rotations or reflections). The resulting set of all closed loops, or fermion bilinears, modulo lattice symmetries is denumerable but remains infinite, even on a finite lattice of just one plaquette. So the challenge is to formulate an effective variational strategy for this infinite dimensional minimization problem.

Any practical numerical calculation will necessarily involve some truncation of the variational domain to a finite dimensional subdomain. One simple approach is to select, in some manner, a finite set of Wilson loop expectations (and fermion bilinears) and simply neglect — approximate by zero — all other expectations not in the retained set. This will be referred to as a “loop list” truncation scheme.

In the infinite coupling limit, expectation values of all Wilson loops vanish identically, $W_\Gamma = 0$, except for the trivial identity “loop” which goes nowhere and has unit holonomy. For large but finite values of the lattice gauge coupling $\lambda \equiv g^2 N$, Wilson loop expectation values are non-zero but small, with a hierarchy of sizes determined by the order in a strong coupling expansion (i.e., a Taylor series in $1/\lambda$) at which a given loop first acquires a non-zero expectation. So, at least for sufficiently strong coupling, a truncation scheme which neglects expectation values of all observables outside some set of selected observables can work well, especially if the selection of retained observables is directly based on the strong coupling order at which different loops first acquire expectation values. How to perform such a selection is described below.

The downside of using a state representation based on the neglect of expectation values of observables outside some finite (perhaps large) set of retained Wilson loops is that the truncation error produced by neglect of non-retained loop expectations necessarily grows as the lattice gauge coupling decreases, since the correct expectation value of any fixed Wilson loop tends to unity in the weak coupling limit. So this type of state representation will have a domain of utility which extends downward from strong coupling but terminates at some non-zero value of the coupling when observable truncation errors become too large to ignore. How this domain of utility depends on the size of the truncation set, and whether it can extend into the weak coupling regime of the theory for sufficiently large truncations, can only be answered by doing the requisite calculations and examining results.

An alternative approach for representing, and truncating, the information defining a particular gauge theory coherent state is provided by large- N “master fields”. In the $N \rightarrow \infty$ limit, one can argue that a single gauge field configuration can reproduce all Wilson loop expectation values [24–26]. On a translationally invariant lattice, any master field realization must also be translationally invariant up to a gauge transformation. Without loss of generality, one may choose a realization in which the link matrices are translation invariant

without any additional gauge transformation. For a d -dimensional simple cubic lattice, this means that a set of just d unitary matrices, $\{u_i\}$, $i = 1, \dots, d$, in the limit in which the size of these matrices tends to infinity, can lead to holonomies whose traces exactly reproduce all large- N Wilson loop expectation values. In effect, one is using unboundedly large matrices to encode an unboundedly large amount of information. By introducing additional matrices to represent electric field insertions or fermions, this master field approach can be extended to handle the gauge field conjugate momenta (2.2) and fermion bilinears (2.4) [2].

The master field formulation suggests an obvious alternative truncation strategy for approximate numerical calculations: simply restrict master field matrices to some large but finite size. Then use ordinary matrix multiplication to evaluate the (truncated approximation) to any Wilson loop or fermion bilinear expectation value. However, no finite-dimensional set of unitary matrices can reproduce the correct large- N expectation values of all Wilson loops in the infinite coupling limit.

Choosing the gauge field master field approximations $\{u_i\}$ to be independent random $K \times K$ unitary matrices provides, in the limit that $K \rightarrow \infty$, a valid master field realization for the ground state at infinite gauge coupling. But for finite K , any particular realization of d such random $U(K)$ matrices will generically lead to non-vanishing values for the trace (divided by K) of the product of these matrices around any closed loop, with both the mean and variance of the resulting normalized random matrix loop trace vanishing with increasing matrix rank only as $O(1/K^2)$. The typical error in the approximation to the correct infinite coupling answer of zero only decreases as the square root of this variance, namely linearly with $1/K$. This is awfully slow convergence. One can engineer alternative sequences of finite dimensional approximations to an infinite coupling unitary master field which force traces of certain select classes of loops to exactly vanish. But, even in a lattice theory with only a single plaquette, no set of finite rank unitary master field approximations can correctly reproduce all Wilson loop expectations at infinite coupling.⁹

Hence, at least in the strong coupling regime, a state representation based on finite size master field approximations will have greater truncation error than a state representation using a comparably sized loop-list truncation. But a state representation using some approximate master field provides, by construction, a valid unitary gauge field configuration. Such an approximation will automatically satisfy all (rank-independent) positivity constraints, such as the trivial bound $|W_\Gamma| \leq 1$. As will be discussed further below, respecting such positivity constraints is non-trivial when using a truncated loop-list state representation.

Clearly, different truncation schemes for the state representation will have differing pros and cons. Properly assessing the utility of either of the above approaches requires fully implementing a variational procedure using a given truncation scheme, applying this procedure with different sized truncations to various theories, and examining results. This

⁹ Formulating some reasonable notion of optimality for a finite-dimensional master field approximation, just at infinite gauge coupling, or constructing specific approximations which are, in some meaningful sense, superior to random unitaries, are interesting problems which have received little attention.

paper presents work using state representations involving a finite truncated list of physical expectation values. A future work will examine the alternative master field based approach.

Within the loop-list class of truncation schemes, a key question is how to select those observables whose expectation values will be retained. Classifying loops based on their length is a particularly simple scheme, but in the strong coupling domain of a lattice gauge theory the most effective truncation scheme — essentially by definition — involves classifying Wilson loops according to their *strong-coupling order*. This is defined as the order in a strong coupling expansion of the ground state energy (or Euclidean free energy) at which an error is first made if the particular loop’s expectation value is omitted from an otherwise correct expansion. As shown in Ref. [3], the strong-coupling order of a Wilson loop is the sum of its *creation order* plus *expectation order*. The creation order is defined as twice the number of nested commutators involving a single plaquette with one electric field insertion acting on an initial single plaquette which are needed to generate a given loop, while the expectation order is twice the number of such single plaquette commutations required to return the loop in question to the identity. These two orders can differ due to the unitary nature of the gauge field and consequent automatic cancellation of backtracking links which can occur in the latter process. This approach can be extended to Wilson loops with electric field insertions, as well as fermion bilinears; see Ref. [3] for details.¹⁰

So a state representation based on storing a finite subset of Wilson loop expectation values, with a selection criterion based on an observable’s strong-coupling order, provides a highly effective representation of the properties of a large- N coherent state in the large gauge coupling (and large fermion mass) regime of the theory. There is, of course, no guarantee that the same observable truncation scheme will continue to provide an effective approximate state representation in the weak coupling regime. But, simply put, no clearly superior computationally useful representation is known today, and the only way to determine the limit of utility of this approach is to put it into practice and examine results.

¹⁰ When fermions are present in the theory, the classification is based on a simultaneous strong coupling and large mass expansion, and the creation order is defined as the minimal sum of the number of commutations with single-link fermion hopping terms plus twice the number of commutations with single plaquette generators needed to produce the given observable. The expectation order is equal to the minimal sum of the number of commutations with single-link fermion hopping terms plus twice the number of commutations with single plaquette generators needed to yield the identity operator, or a single-site fermion bilinear, starting from the given observable. If there are compactified directions, see Ref. [3] for precise definitions. These definitions of observable creation, expectation, and strong-coupling orders are all twice those used in Ref. [3], so as to avoid half-integral creation or expectation orders for fermion bilinears. The counting of plaquette operations with double the weight of fermion hopping operations reflects the structure of the standard Kogut-Susskind Hamiltonian [6]. In H/λ , the gauge kinetic energy is $O(1)$ while the fermion kinetic energy (or hopping term) is $O(1/\lambda)$ and the gauge potential energy (or plaquette term) is $O(1/\lambda^2)$.

B. Variational parameters

The next essential ingredient in any variational minimization is the choice of variational parameters; what gets varied to move around in the minimization domain? The most typical (and obvious) choice is to identify one's variational parameters with whatever is providing the state representation. In other words, to use Wilson loop (and fermion bilinear) expectation values themselves as variational parameters. For large- N gauge theories, this is a bad choice, for at least two independent reasons:

First, traces of holonomies (i.e., Wilson loops) necessarily satisfy an intricate set of inequalities. The most basic is just $|W_\Gamma| \leq 1$, but there are infinitely many more inequalities relating different traces which follow just from unitarity.¹¹ As a result, if Wilson loop expectation values are viewed as coordinates on the large- N classical phase space, then the physical domain has a highly non-trivial boundary arising at finite values of these coordinates. Moreover, as the lattice gauge coupling is varied (and decreased), the minimum of the large- N Hamiltonian can move from the interior of the physical domain toward the boundary, hit the boundary at some critical value of gauge coupling, and thereafter move within the physical domain boundary. This is one way to understand the origin of the third-order large- N phase transition in one-plaquette models [31, 32, 35]. It is quite awkward to formulate an effective numerical minimization algorithm which can handle, correctly, the desired minimum reaching and then moving along this non-trivial boundary surface.

The second problem is that the functions one wants to minimize, namely the classical Hamiltonian (defined as the coherent state expectation of the quantum Hamiltonian, rescaled by N^{-2}) or, for the Euclidean formulation, the free energy (1.1) of a coherent state ensemble (also rescaled by N^{-2}), do not have simple expressions in terms of Wilson loop expectation values. The standard Kogut-Susskind lattice Hamiltonian,

$$H_{\text{gauge}}/N = \frac{1}{4}\lambda \sum_\ell \text{tr}(E_\ell^2) + \lambda^{-1} \sum_p \text{tr}(2 - U_{\partial p} - U_{\partial p}^\dagger), \quad (2.5)$$

is a sum of kinetic energy, proportional to $\sum_\ell \text{tr} E_\ell^2$, and potential energy, depending on the sum of single plaquettes, $\sum_p \text{tr} U_{\partial p}$ (with $U_{\partial p}$ denoting the holonomy around the boundary of plaquette p). The kinetic energy expectation value, in time-reversal invariant states, can be formally expressed in terms of Wilson loop expectation values, but the result is far from computationally convenient. One may show that [1]

$$\lim_{N \rightarrow \infty} \frac{1}{N} \sum_\ell \langle \text{tr}(E_\ell^2) \rangle = \sum_{\Gamma, \Gamma'} \omega_\Gamma (\Omega^{-1})_{\Gamma\Gamma'} \omega_{\Gamma'}, \quad (2.6)$$

where the double sum runs over the complete set of all possible closed loops.¹² The “loop-

¹¹ For example [13], $|W_\Gamma - W_{\Gamma'} W_{\Gamma''}|^2 \leq (1 - |W_{\Gamma'}|^2)(1 - |W_{\Gamma''}|^2)$ for any the self-intersecting loop Γ with sub-loops Γ' and Γ'' , such that $\Gamma = \Gamma'\Gamma''$.

¹² In time reversal non-invariant coherent states, there is an additional term involving a quadratic form in

joining” matrix Ω has components

$$\Omega_{\Gamma\Gamma'} \equiv \lim_{N \rightarrow \infty} N \sum_{\ell} \langle [\text{tr } U_{\Gamma}, (E_{\ell})_{ij}] [(E_{\ell})_{ji}, \text{tr } U_{\Gamma'}] \rangle, \quad (2.7)$$

while the “loop-splitting” vector ω has components

$$\omega_{\Gamma} \equiv \lim_{N \rightarrow \infty} \sum_{\ell} \langle [(E_{\ell})_{ij}, [(E_{\ell})_{ji}, \text{tr } U_{\Gamma}]] \rangle. \quad (2.8)$$

For any pair of loops Γ and Γ' , the loop-joining matrix element $\Omega_{\Gamma\Gamma'}$ is a linear combination of Wilson loops which result when Γ and Γ' are sewn together at some commonly-traversed link ℓ . Similarly, each component ω_{Γ} of the loop-splitting vector is a linear combination of the original loop Γ and quadratic products of subloops which result when the loop Γ is split apart at some multiply-traversed link ℓ .

A key point is that the quadratic form (2.6) involves components of the inverse loop-joining matrix, Ω^{-1} , i.e., the inverse of an infinite dimensional matrix. One finds in simple models, and can argue more generally, that the loop-joining matrix Ω is insufficiently diagonally dominant for a truncation to a finite set of loops of its inverse to be well approximated by the inverse of its truncation to that finite set. (I.e., the inversion of a truncation provides a poor approximation to the corresponding truncation of the true inverse.) So, despite the validity of the formal result (2.6), expressing the gauge field kinetic energy in terms of Wilson loop expectations in some computationally useful form is very problematic.

An entirely analogous issue arises in the Euclidean formulation, where the free energy (1.1) depends on the entropy of a statistical ensemble of interest. In the large N limit, that entropy is, in principle, expressible in terms of Wilson loop expectations. But, just as with the gauge kinetic energy in the Hamiltonian formulation, there is no explicit computationally useful formula.¹³

For both the above reasons, Wilson loop expectations fail to serve as good variational parameters. The alternative adopted in the coherent state variational algorithm of Refs. [2, 3] takes advantage of the intrinsic geometry of the large N phase space (or manifold of coherent states) which follows from the underlying structure of the infinite dimensional *coherence group* \mathcal{G} which generates gauge theory coherent states.

The coherence group \mathcal{G} consists of unitary operators exponentiating elements (or genera-

which the canonical conjugates of Wilson loops are doubly contracted with the loop-joining matrix Ω .

¹³ The Migdal-Makeenko loop equations [15], an infinite set of polynomial equations satisfied by large- N Euclidean Wilson loop expectations, are a formulation of the conditions defining a saddle-point of the large- N free energy. For computational purposes, it is vastly preferable to have a variational formulation with a computable free energy, bounded below, which one is minimizing. The loop equations themselves can have multiple solutions (even within the physical domain) corresponding to multiple saddle points of the free energy. Knowledge of the free energy is required to identify the correct physical solution.

tors) of the *coherence Lie algebra* \mathbf{g} ,

$$\mathcal{G} \equiv \{e^\Lambda \mid \Lambda \in \mathbf{g}\}. \quad (2.9)$$

For QCD-like theories, elements of this infinite dimensional Lie algebra are anti-Hermitian linear combinations of arbitrary Wilson loops, loops with one electric field insertion, and fermion bilinears,¹⁴

$$\mathbf{g} \equiv \{\Lambda(a, b, c)\}, \quad (2.10)$$

with

$$\Lambda(a, b, c) \equiv \sum_{\Gamma} N a_{\Gamma} \text{tr}(U_{\Gamma}) + \sum_{\ell, \Gamma} N b_{\ell, \Gamma} \text{tr}(E_{\ell} U_{\Gamma}) + \sum_{\Gamma_{xy}} c_{\Gamma_{xy}} \bar{\psi}_x U_{\Gamma_{xy}} \psi_y. \quad (2.11)$$

Elements of \mathcal{G} acting on a base state (which may be taken to be the infinite gauge coupling, infinite fermion mass ground state) generate the manifold of coherent states which, collectively, form a *coadjoint orbit* of \mathcal{G} [1, 3].

As in any Lie group, one parameter subgroups formed by exponentiating some given Lie algebra element, $e^{s\Lambda(a,b,c)}$ for $\Lambda(a, b, c) \in \mathbf{g}$ and $s \in \mathbb{R}$, are geodesics on the group manifold. Elements of \mathcal{G} which lie in a neighborhood of the identity, when acting on any given coherent state $|u\rangle$, generate coherent states lying in a neighborhood of $|u\rangle$. Consequently, when a coherence group element $e^{\Lambda(a,b,c)}$ acts on a coherent state $|u\rangle$, the Lie algebra coefficients $\{a_{\Gamma}, b_{\ell, \Gamma}, c_{\Gamma_{xy}}\}$ are precisely *Riemann normal coordinates*, and parameterize coherent states in the neighborhood of $|u\rangle$. Most importantly, such Riemann normal coordinates may serve as variational parameters in an iterative minimization scheme.

If, at some point in the iterative minimization, one wishes to move from a coherent state $|u\rangle$ to some nearby state $|u'\rangle \equiv e^{\Lambda(a,b,c)}|u\rangle$, then the change in the expectation value of any observable \mathcal{O} may be computed by integrating the *geodesic equation*,

$$\frac{d}{ds} \langle \mathcal{O} \rangle_s = \langle [\mathcal{O}, \Lambda(a, b, c)] \rangle_s \quad (2.12)$$

from $s = 0$ to $s = 1$. Here, $\langle \cdots \rangle_s$ denotes an expectation value in the intermediate states $\{|u(s)\rangle \equiv e^{s\Lambda(a,b,c)}|u\rangle\}$ which comprise the geodesic connecting $|u\rangle$ to $|u'\rangle$. The key point is that, for observables of interest, the commutator defining this geodesic equation can be evaluated analytically using the underlying lattice gauge theory commutation relations. In particular, because coherence group generators contain at most one electric field insertion, the derivative along a geodesic of any Wilson loop expectation is some linear combination of other Wilson loop expectations. Similarly, the derivative of any fermion bilinear is a linear combination of other fermion bilinears.

Actually evaluating, explicitly, the commutators defining the geodesic equations (2.12) for

¹⁴ This is the Hamiltonian theory description. See Ref. [3] for the appropriate normal-ordering specifications, and for discussion of the parallel Euclidean formulation.

a large (but finite) set of Wilson loops and/or fermion bilinears and a large set of coherence group generators can be a major undertaking, but this symbolic computation task, for a given set of observables and generators, need only be performed once.

This approach of using Riemann normal coordinates as variational parameters bypasses the problem of inequality violations which arises when Wilson loop expectations are used directly as variational parameters. Deformations in a coherent state produced by the action of a coherence group element necessarily leave the state within the physical domain.¹⁵

The second problem discussed above, namely the computability of the gauge kinetic energy or entropy, can also be dealt with in this approach by augmenting the set of observables used in the state representation. In the Euclidean formulation this is simple, one must merely add the entropy to the set of retained Wilson loops. The geodesic equations for the entropy are easily expressed in terms of Wilson loop and/or fermion bilinear expectations [3]. For example, the entropy variation induced by the gauge generator $\Lambda(0, b, 0)$ is given by

$$\delta(S/N^2) = -\frac{1}{N} \sum_{\ell, \Gamma} b_{\ell, \Gamma} \langle \text{tr} [E_\ell, U_\Gamma] \rangle. \quad (2.13)$$

Evaluating this single trace “internal” commutator leads to a quadratic polynomial in Wilson loop expectations.

In the Hamiltonian formulation, a commutator of the gauge kinetic energy with a coherence group generator (2.11) leads to linear combinations of expectations of Wilson loops with one electric field insertion, Wilson loops with two electric field insertions, and fermion bilinears with one electric field insertion.¹⁶ Therefore, to make it possible to integrate the variation of the kinetic energy along a geodesic, it is necessary to include Wilson loops with up to two electric field insertions and fermion bilinears with one electric field insertion in the set of retained observables. As noted earlier, the classification of observables according to their strong-coupling order can be extended in a straightforward manner to loops or bilinears containing electric field insertions.

These additional observables with electric field insertions are, in time-reversal invariant states, redundant variables which could, in principle but not in practice, be expressed in terms of Wilson loop and fermion bilinear expectation values. By adding them explicitly to the set of retained observables, all geodesic variations become computable polynomials in expectation values of those observables.

¹⁵ This, of course, presumes that errors induced by a truncated state representation are under control.

With a loop-list state representation, when integrating the (truncated) geodesic equations, the resulting expectations may eventually violate positivity bounds when the truncation error in the state representation becomes significant. This can serve as a useful diagnostic for the limit of utility of a given truncation.

¹⁶ As explained in Ref. [3], in the commutator of a single- E generator with a double- E Wilson loop, the normal-ordering prescriptions also lead to terms cubic in Wilson loops.

C. Coherent state variational algorithm

The above choices of state representation and variational parameters lead directly to the coherent state variational algorithm as formulated in Ref. [3]. The basic steps are:

1. Construction of a list of observables $\{\mathcal{O}_i\}$ of the chosen theory to be retained in the finite truncation set, and whose expectation values will be computed. In Euclidean theories, “observables” mean Wilson loops and fermion bilinears, plus the entropy, while in Hamiltonian theories observables are Wilson loops with up to two electric field insertions and fermion bilinears possibly with one electric field insertion.
2. Selection of the finite set $\{e_\alpha \in \mathbf{g}\}$ of coherence group generators, for a given theory, which will be used to generate deformations of coherent states, and whose coefficients will serve as Riemann normal coordinates in the neighborhood of any given point in the large N phase space. These are anti-Hermitian combinations of Wilson loops (in Hamiltonian theories), loops with one electric field insertion, and fermion bilinears.
3. Symbolic evaluation of the commutators of selected observables and generators. These define the geodesic equations on the large N phase space, encoding how observables vary as one deforms the state,

$$\frac{d}{ds} \langle \mathcal{O}_i \rangle = \sum_{\alpha} c^{\alpha} \langle [\mathcal{O}_i, e_{\alpha}] \rangle. \quad (2.14)$$

4. Symbolic evaluation of the commutators defining the first and second variations of the Hamiltonian (or Euclidean free energy) with respect to Riemann normal coordinates,

$$(dH)_{\alpha} \equiv \langle [H, e_{\alpha}] \rangle, \quad (d^2H)_{\alpha\beta} \equiv \langle [[H, e_{\alpha}], e_{\beta}] \rangle. \quad (2.15)$$

And for Hamiltonian theories, evaluation of commutators of generators whose resulting expectation values define the Lagrange bracket (or inverse Poisson bracket) of the large N phase space,

$$L_{\alpha\beta} \equiv \langle [e_{\alpha}, e_{\beta}] \rangle. \quad (2.16)$$

5. Numerical minimization of the Hamiltonian, or Euclidean free energy, using Newton iteration. Each iterative step involves numerical evaluation of the symbolic expressions for the gradient and curvature of the Hamiltonian (or free energy), followed by solution of the linear equations predicting the location of the minimum,

$$c \equiv -(d^2H)^{-1} \cdot (dH). \quad (2.17)$$

and numerical integration of the geodesic equations describing the change in expectation values of all observables as one moves to the newly predicted minimum.

6. In Hamiltonian theories, numerical evaluation of the symbolic expressions for the curvature of the Hamiltonian and the Lagrange bracket, in any chosen symmetry channel, and evaluation of the resulting small oscillation frequencies around the minimum yielding a determination of the low-lying glueball or meson spectrum. This requires solving the generalized eigensystem

$$(d^2 H) \cdot \delta = i\omega L \cdot \delta. \quad (2.18)$$

Each of these steps is carried out first for the $O(N^2)$ pure gauge dynamics, and then again for the sub-leading $O(N)$ fundamental representation fermion dynamics.

D. Why bother?

Before describing the recent (re)implementation of the coherent state variational method, and presenting initial results from this implementation, it may be worthwhile to address a very basic question: given all the advances in stochastic simulations of Euclidean lattice gauge theories over the past four decades, including work exploring N dependence by running simulations with progressively larger values of the gauge group rank [7–12], is an effort to solve, numerically, for properties of QCD-like gauge theories directly at $N = \infty$ worth the trouble? Although only classical minimization is involved, with no stochastic sampling, it is evident that minimizing the Hamiltonian of the large- N classical dynamics (or free energy of the large- N statistical mechanics) is a hard problem, surely exponentially hard in terms of dependence on correlation length.

From the outset, it is clear that coherent state studies of QCD at $N = \infty$ will not compete with evaluations of experimentally observable quantities (such as light hadron masses and selected weak matrix elements) for which it is already feasible to achieve fully-controlled percent-level accuracy in Euclidean lattice simulations of real ($N = 3$) QCD. If the only potential output from numerical work directly studying the $N = \infty$ limit of lattice Yang-Mills theory were, say, the ground state energy density and expectation values of a few small Wilson loops, it would be hard to justify the effort. But that is too narrow a perspective. Reasons for pursuing numerical studies of large N Yang-Mills and QCD, despite the inherent difficulty, include the following:

- The ability to study lattice gauge theories in a Hamiltonian formulation. The Euclidean formulation of the coherent state variational method is a desirable variant which can enable direct comparison with Euclidean lattice simulations, but it is the Hamiltonian formulation which is of most interest.
- The ability to work directly in infinite volume is also a key feature which distinguishes the large N coherent state approach from Euclidean lattice simulations.
- The ability to easily study theories with dynamical fermions, without any of the complications needed for dealing with the Dirac determinant in lattice simulations.

- Extracting from lattice simulations the spectrum of hadronic resonances (especially glueballs) which decay via strong interactions is challenging, whereas in the Hamiltonian formulation of large N dynamics this merely requires the evaluation of small oscillation frequencies about the minimum of the large N classical Hamiltonian.
- While there has been notable recent progress on the extraction of scattering amplitudes from Euclidean lattice simulations [21, 22], doing so is extremely challenging and currently only feasible in limited cases. The potential to extract decay widths and scattering amplitudes from third and fourth derivatives of the large N classical Hamiltonian (with no finite size effects or momentum quantization constraints to contend with) is a novel feature. This capability has not yet been implemented, as it requires evaluation of commutators of operators with non-zero momentum, but is a feasible extension of current work and a significant motivation for the approach.
- The large N limits of Yang-Mills and QCD-like theories are intrinsically interesting in their own right. Performing classical minimization of the large N Hamiltonian, despite the difficulty, is surely far more achievable than using any foreseeably existing quantum computer to perform real time evolution and extraction of, say, the glueball spectrum in infinite volume 2+1 or 3+1 dimensional Yang-Mills theory.

III. THE PROGRAM “GORDION”

Early work in the 1980’s [2, 3, 27–29] found that the coherent state variational approach works well in simple test cases. In non-trivial higher dimensional lattice gauge theories the approach, by design, works well at sufficiently strong coupling. But as the gauge coupling decreases and the correlation length grows, it is inevitable that at some point any given truncation will cease to provide a good approximation. With the computing resources available in the 1980’s, it was not really feasible to reach values of the lattice gauge coupling where one would begin to see weak-coupling behavior.

Computing capabilities have, of course, vastly increased since the 1980’s. Might it now be possible to obtain decent results at interestingly small values of the gauge coupling in non-trivial large- N lattice gauge theories? The only way to find out is to try. This motivated the decision to create a unified program, efficiently written, which can carry out all the steps in the coherent state variational algorithm in a variety of lattice gauge theories of interest.

The program name *Gordion* is an allusion to the Greek legend associated with Alexander the Great, who is reputed to have sliced through a horrendously complicated knot, instead of carefully untying it, in Gordion (Latin: Gordium, Phrygian: Gordum), the capital city of ancient Phrygia. Dealing with arbitrarily complicated loops is, of course, at the core of the coherent state variational method as applied to lattice gauge theories.

The design goal was creation of a program capable of handling $U(N)$ gauge theories on translationally invariant cubic lattices in dimensions ranging from 1 up to 4, in either Hamil-

tonian or Euclidean formulations, with or without fundamental representation fermions. More specifically:

- The lattice dimension may be 1, 2, 3 or 4, with each dimension either infinite, or periodically compactified.
- Zero, one or two fermion flavors are allowed, with each fermion flavor defined as having one conjugate pair of fermion operators per site per flavor.
- All theories under consideration are invariant under cubic lattice symmetries (translations, permutations, and reflections) together with charge conjugation (C) and time reversal.¹⁷
- None of these symmetries are spontaneously broken, and observables of interest are invariant under all symmetries.

The current program includes evaluation of the curvature of the Hamiltonian and extraction of small oscillation frequencies in any chosen point group representation, but only for translationally invariant (zero momentum) excitations. The program design also allows testing a factorization-based observable approximation scheme as discussed below in Sec. V.

Extending the code to handle spectrum calculations at non-zero momentum is a potential future addition, as are calculations of decay widths or scattering amplitudes requiring evaluation of higher derivatives about the minimum of the large- N classical Hamiltonian.

The implementation language is C++. This choice, instead of some higher level programming language, allows a substantially more efficient implementation. The program effectively uses multi-core processors and parallelizes the major time-consuming steps in the approach including observable generation, commutator evaluation for geodesic equations, and numerical evaluation of geodesic equations. Although compute capabilities have vastly increased since the 1980's, the computational complexity of numerically minimizing the large N Hamiltonian (or Euclidean free energy) to a given accuracy inevitably grows exponentially with the correlation length of the theory, since the number of Wilson loops grows exponentially with any reasonable measure of their size. Because the continuum limit entails diverging correlation length, for any given level of computational resources a more efficient implementation will allow one to reach larger correlation lengths.

As described above, the first step in applying the coherent state variational method, using a loop-list truncation scheme, involves the generation of all relevant observables with strong coupling orders below some specified limit. Using the new program, Table I shows the resulting number of “canonicalized” gauge observables (i.e., counting as a single observable all those related by any symmetry) with 0, 1 or 2 electric field insertions as a function of

¹⁷ When fermions are present, the size of any compactified dimension must be an even number of lattice spacings and, in Hamiltonian theories, only translations by an even number of lattice spacings are symmetries of the theory.

strong-coupling order	2D lattice			3D lattice			4D lattice
	Loop	<i>E</i> -loop	<i>EE</i> -loop	Loop	<i>E</i> -loop	<i>EE</i> -loop	Loop
0	1	-	-	1	-	-	1
4	1	2	1	1	2	1	1
8	3	7	20	5	13	48	5
12	17	102	506	63	431	1,939	78
16	196	2,524	19,597	2,134	28,871	213,759	3,509
20	3,989	75,952	888,217	142,093	2,519,588	28,394,853	349,740
24	109,454	2,542,659	40,684,963	11,992,955	250,454,123	$> 2^{32}$	45,996,638
28	3,380,056						
32	111,958,945						

TABLE I. Counts of canonicalized gauge observables of the indicated types and specified strong-coupling order, on cubic lattices of dimension 2, 3 or 4.

their strong-coupling order and lattice dimension.¹⁸ These observable sets extend to strong coupling orders well beyond what was possible to generate in earlier work [3].

Much more information about the program *Gordion* may be found in the design and implementation notes [30]. These notes, together with the program code itself, are available on the Github repository. Interested readers are encouraged to download the program, read the program notes, and give it a try.

IV. RESULTS

Models with exactly soluble large- N limits, in both Euclidean and Hamiltonian formulations, provide instructive testing grounds for any approach to large- N dynamics which may have more general applicability. The performance of the coherent state variational algorithm for one-plaquette models was examined in Refs. [2, 3]. That examination is briefly repeated here, both to show a check on the correctness of the new implementation of the method and to illustrate the impact of different truncations of coherence group generators. Following this, results are presented for two-dimensional Euclidean Yang-Mills theory on an infinite lattice, without using the non-local change of variables which allows one to reduce the theory to a product of decoupled single-plaquette models. This is a far more demanding test case which allows one to study effects of observable and generator truncations with the

¹⁸ More detailed counts of observables with specified creation and expectation orders may be found in the implementation notes [30]. For pure loop observables, the counts shown in table I agree with those shown in tables 1–3 of Ref. [3] for strong-coupling orders below 24 (labeled as order 12 in Ref. [3]), but there are discrepancies at order 24, the highest order reported in Ref. [3], with undercounts in the older reference. The reason for this discrepancy with old results is not known. For observables with electric field insertions, there are more extensive discrepancies with the old results. This, it is believed, reflects a subtlety involving the expectation order determination for such observables; see footnotes 10 and 11 in the notes [30].

full complexity of a multi-dimensional lattice. Finally, initial results are presented for 2+1 dimensional Hamiltonian Yang-Mills theory.

A. Euclidean one-plaquette model

The Euclidean one-plaquette model is defined by the probability measure

$$d\mu[U] \equiv Z^{-1} e^{-A[U]} dU, \quad (4.1)$$

where dU denotes Haar measure on $U(N)$ and the action

$$A[U] \equiv \frac{N}{\lambda} \text{tr} (2 - U - U^\dagger). \quad (4.2)$$

The partition function normalizing the measure is defined as usual, $Z \equiv \int dU e^{-A[U]}$. The free energy $F \equiv -\ln Z$, and the entropy $S \equiv \langle A \rangle - F$, with $\langle A \rangle \equiv \int d\mu[U] A[U]$.

The large- N limit may be solved by diagonalizing the matrix U and then performing a saddle-point expansion of the resulting integral over eigenvalues [31]. One finds a density of eigenvalues

$$\rho_0(\theta) = \begin{cases} 1 + \frac{2}{\lambda} \cos \theta, & \lambda \geq 2; \\ \frac{4}{\lambda} \cos \frac{\theta}{2} (\frac{\lambda}{2} - \sin^2 \frac{\theta}{2})^{1/2} \Theta(\frac{\lambda}{2} - \sin^2 \frac{\theta}{2}), & \lambda \leq 2, \end{cases} \quad (4.3)$$

where $\Theta(z)$ is the unit step function. The large- N expectation value of the unit winding Wilson loop is given by

$$w_1 \equiv \lim_{N \rightarrow \infty} \int d\mu[U] \frac{1}{N} \text{tr} U = \int \frac{d\theta}{2\pi} \rho_0(\theta) \cos \theta = \begin{cases} \frac{1}{\lambda}, & \lambda \geq 2; \\ 1 - \frac{\lambda}{4}, & \lambda \leq 2, \end{cases} \quad (4.4)$$

while higher winding-number $k > 1$ loops have expectation values

$$\begin{aligned} w_k \equiv \lim_{N \rightarrow \infty} \int d\mu[U] \frac{1}{N} \text{tr} U^k &= \int \frac{d\theta}{2\pi} \rho_0(\theta) \cos(k\theta) \\ &= \begin{cases} 0, & \lambda \geq 2; \\ (1 - \frac{\lambda}{2}) \left[\frac{P'_k(1-\lambda)}{k(k+1)} + \frac{P'_{k-1}(1-\lambda)}{k(k-1)} \right], & \lambda \leq 2, \end{cases} \end{aligned} \quad (4.5)$$

with $P'_m(z)$ the derivative of the Legendre polynomial of order m . The resulting large- N free energy is given by

$$f \equiv \lim_{N \rightarrow \infty} F/N^2 = \begin{cases} \frac{2}{\lambda} - 1/\lambda^2, & \lambda \geq 2; \\ \frac{3}{4} - \frac{1}{2} \ln \frac{\lambda}{2}, & \lambda \leq 2, \end{cases} \quad (4.6)$$

and possesses a third-order large- N phase transition at $\lambda = 2$. Finally, the large- N entropy

$$s \equiv \lim_{N \rightarrow \infty} S/N^2 = \frac{2}{\lambda} (1 - w_1) - f. \quad (4.7)$$

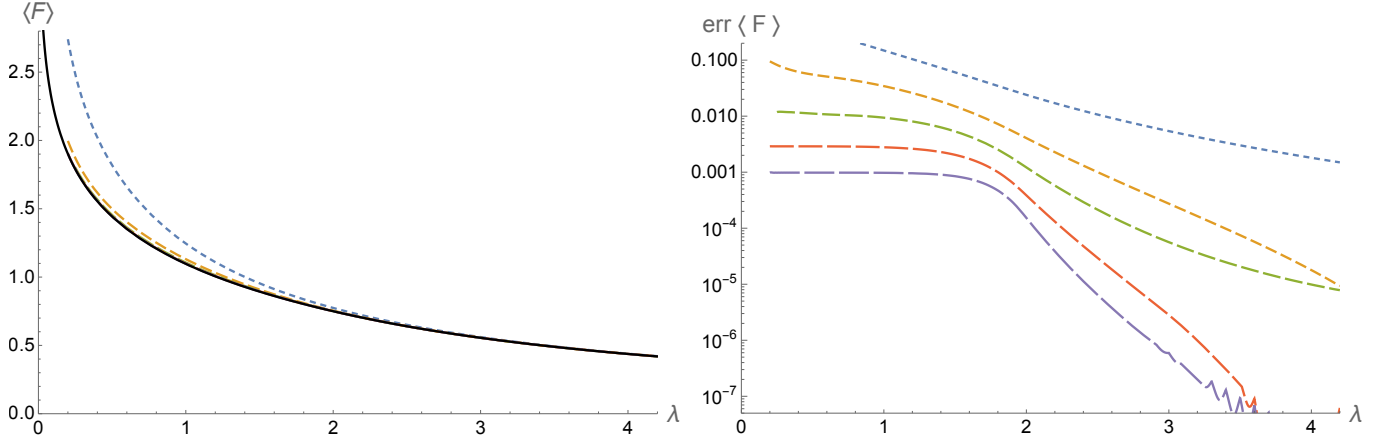


FIG. 1. Left: Free energy of the Euclidean one-plaquette model. Shown is the exact result (solid black line) and results from variational calculations using 1 through 5 generators. Results with three or more generators are not visually distinguishable from the exact curve. Right: Semi-log plot of the absolute error magnitude between exact and variational results with 1 (blue), 2 (orange), 3 (green), 4 (red), or 5 (purple) generators; curves with progressively longer dashes have an increasing number of generators.

Applying the coherent state variational algorithm to this model is straightforward. Within the framework of the program *Gordion*, this theory is viewed as living on a one-dimensional lattice periodically compactified to a single lattice spacing. The link variable U is the Polyakov loop around this compact direction. The strong-coupling order of a winding- k loop, as defined earlier, is just four times the winding number.

Figure 1 shows a plot of the exact large- N free energy f together with the results from variational calculations using coherence group generators $\text{tr}(EU^k)$ with maximal windings ranging from 1 up to 5. Figure 2 shows a similar plot for the unit winding loop expectation w_1 , while Fig. 3 shows results for the winding three expectation w_3 .¹⁹ The left hand side of these figures illustrate the approach of the variational approximations to the exact results as the number of generators increases. The logarithmic error plots on the right hand side of these figures display the magnitudes of absolute errors between the exact results and the progressively improving variational approximations.

The phase transition at $\lambda = 2$ is not visually apparent in the left-hand plots of the free energy or winding-one loop expectation w_1 , and results with three generators for these

¹⁹ In all cases, loops with sufficiently high winding numbers are retained so that observable truncation error is negligible. Except at rather weak coupling, retaining two to three times the number of observables as generators is sufficient. But for couplings well below 1, the curvature matrix becomes increasingly poorly conditioned due to very small eigenvalues. This causes observable truncation effects to become more significant, with substantially larger truncations required to obtain good results. The development of a nearly singular curvature matrix is a consequence of the eigenvalue distribution (4.9) becoming increasingly peaked around the identity. This causes the actions of winding- k generators on the eigenvalue distribution, given by $\delta\rho_0(\theta) \propto \cos k\theta (\partial\rho_0(\theta)/\partial\theta)$, to become ever more nearly linearly dependent.

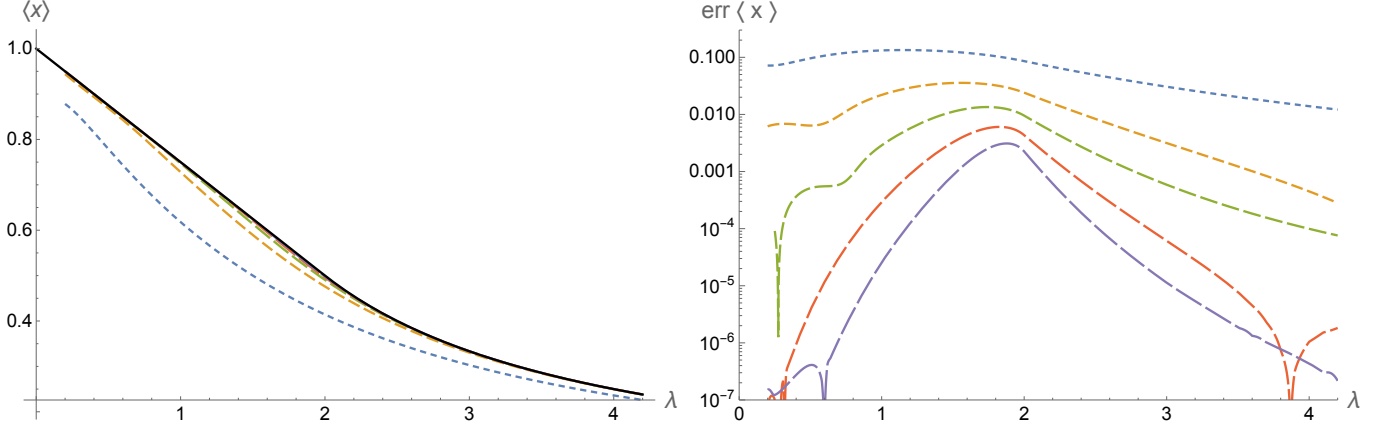


FIG. 2. Left: Winding one loop expectation value $w_1 \equiv \langle x \rangle$ in the Euclidean one-plaquette model. Shown is the exact result (solid black line) and results from variational calculations using 1 through 5 generators. Results with three generators are barely visually distinguishable from the exact curve. Right: Semi-log plot of the absolute error magnitude between exact and variational results with the number of generators ranging from 1 to 5. (The same line styles as in Fig. 1 are used.)

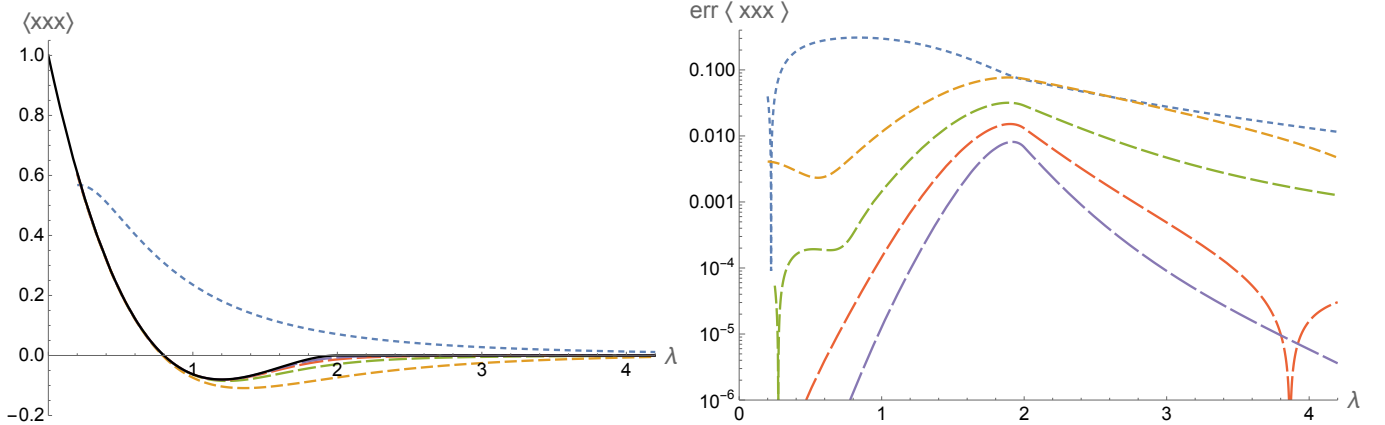


FIG. 3. Left: Winding three loop expectation $w_3 \equiv \langle xxx \rangle$ in the Euclidean one-plaquette model. Shown is the exact result (solid black line) and results from variational calculations using 1 through 5 generators. Results with four generators are barely visually distinguishable from the exact curve. Right: Semi-log plot of the absolute error magnitude between exact and variational results with the number of generators ranging from 1 to 5. (The same line styles as in Fig. 1 are used.)

observables are barely distinguishable from the exact curves. Nevertheless, the error plots on the right do show a clear change in character across the phase transition. For the triply winding loop, whose expectation w_3 exactly vanishes above $\lambda = 2$, the variational results inevitably smooth over the non-analytic behavior at the phase transition. But results with four or more generators deviate only very slightly, just in the immediate neighborhood of the transition, from the exact curve. It is apparent that the variational results converge rather well to the correct large- N limits as the number of generators, and corresponding variational parameters, increases.

B. Hamiltonian one-plaquette model

The Hamiltonian one-plaquette model is defined as

$$H = N \left[\lambda \text{tr} E^2 + \lambda^{-1} \text{tr} (2 - U - U^\dagger) \right], \quad (4.8)$$

where E and U satisfy the specialization of the commutation relations (2.3) to a single link. The large- N limit of this theory may be solved by writing the ground state wavefunction as a function of eigenvalues of the matrix U and then factoring out a Vandermonde determinant of the eigenvalues, which has the effect of converting the Schrodinger equation for eigenvalues into a theory of free fermions [32–34].

One finds a ground state density of eigenvalues given by

$$\rho_0(\theta) = 2\sqrt{e + 2\lambda^{-2} \cos \theta} \Theta(e + 2\lambda^{-2} \cos \theta), \quad (4.9)$$

where e is a Lagrange multiplier enforcing the normalization constraint $1 = \int \frac{d\theta}{2\pi} \rho_0(\theta)$ and $\Theta(z)$ is again the unit step function. When $\lambda > \lambda_c \equiv 8/\pi$ (corresponding to $e > 2/\lambda^2$) the eigenvalue density ρ_0 is strictly positive for all θ , while for $\lambda < \lambda_c$ the density ρ_0 vanishes for some range of angles $|\theta| \geq \theta_{\max}(\lambda)$.

The large- N expectation value of a winding- k Wilson loop is given by

$$w_k \equiv \lim_{N \rightarrow \infty} \left\langle \frac{1}{N} \text{tr} U^k \right\rangle = \int \frac{d\theta}{2\pi} \rho_0(\theta) \cos(k\theta), \quad (4.10)$$

where the final one-dimensional integral must be evaluated numerically. The large- N kinetic energy expectation value may be shown to be given by

$$\lim_{N \rightarrow \infty} \left\langle \frac{1}{N} \text{tr} E^2 \right\rangle = \int \frac{d\theta}{2\pi} \rho_0(\theta)^3, \quad (4.11)$$

and the ground state energy may be expressed as

$$\epsilon_{\text{g.s.}} \equiv \lim_{N \rightarrow \infty} \langle H \rangle / N^2 = 2\lambda^{-1} + \lambda \left[e(\lambda) - \frac{1}{12} - \frac{1}{6} \int \frac{d\theta}{2\pi} \rho_0(\theta)^3 \right]. \quad (4.12)$$

The energy gap, or excitation energy to the lowest excited state, has a finite large- N limit given by [34]

$$\mu \equiv \lim_{N \rightarrow \infty} E_1 - E_0 = \lambda \left[(1 + \Theta(\lambda_c - \lambda)) \int_{-\theta_{\max}(\lambda)}^{\theta_{\max}(\lambda)} \frac{d\theta}{2\pi} \rho_0(\theta)^{-1} \right]^{-1}. \quad (4.13)$$

Excitation energies to higher excited states are just integer multiples of μ [34]. For the k 'th

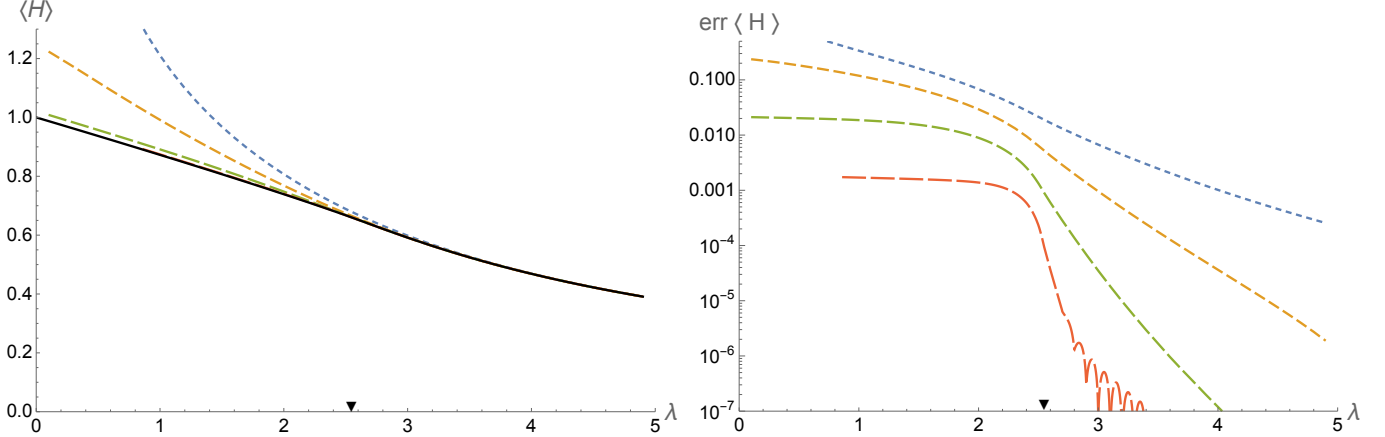


FIG. 4. Left: Ground state energy of the Hamiltonian one-plaquette model. Shown is the exact result (solid black line) and results from variational calculations using 1, 2, 4 and 8 generators. (The eight generator curve is indistinguishable from the exact curve.) Right: Semi-log plot of the absolute error magnitude between exact and variational results with 1 (blue), 2 (orange), 4 (green) and 8 (red) generators; curves with progressively longer dashes have an increasing number of generators. The black triangle on the x -axis marks the position of the phase transition.

even-parity excited state,

$$\delta E_k^+ \equiv \lim_{N \rightarrow \infty} E_k^+ - E_0 = \begin{cases} k \mu, & \lambda > \lambda_c; \\ 2k \mu, & \lambda < \lambda_c, \end{cases} \quad (4.14a)$$

while for the k 'th parity odd excited state,

$$\delta E_k^- \equiv \lim_{N \rightarrow \infty} E_k^- - E_0 = \begin{cases} k \mu, & \lambda > \lambda_c; \\ (2k-1) \mu, & \lambda < \lambda_c. \end{cases} \quad (4.14b)$$

The ground state energy $\epsilon_{\text{g.s.}}$ is only twice-differentiable at $\lambda = \lambda_c$, signaling a third order phase transition. The energy gap μ vanishes at this phase transition in the highly singular fashion,

$$\mu \sim 2\pi (1 + \Theta(\lambda - \lambda_c)) / \ln[\lambda_c / (\lambda - \lambda_c)]. \quad (4.15)$$

Applying the coherent state variational algorithm to this Hamiltonian model is again straightforward. Within the framework of the program *Gordion*, this theory is viewed as living on a one-dimensional spatial lattice periodically compactified to a single lattice spacing, so the link variable U is the spatial Wilson loop around this compact direction.

Figure 4 shows a plot of the exact large- N ground state energy $\epsilon_{\text{g.s.}}$ together with the results from variational calculations using coherence group generators with maximal windings of 1, 2, 4 and 8. Figure 5 shows a similar plot for the unit winding loop expectation w_1 , while Fig. 6 shows results for the winding three expectation w_3 .²⁰ The black triangle on the

²⁰ In all cases, sufficiently many loops are retained so that observable truncation error is negligible.

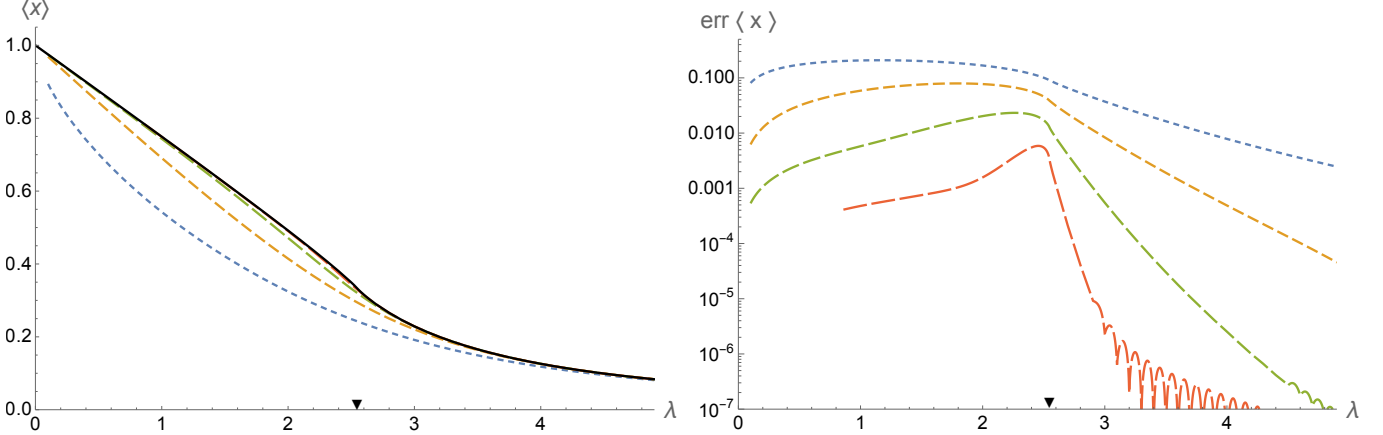


FIG. 5. Left: Single winding loop expectation value $w_1 \equiv \langle x \rangle$ in the Hamiltonian one-plaquette model. Shown is the exact result (solid black line) and results from variational calculations using 1, 2, 4 and 8 generators. (The eight generator curve is indistinguishable from the exact curve.) Right: Semi-log plot of the absolute error magnitude between exact and variational results with 1, 2, 4 and 8 generators. (The same line styles as in Fig. 4 are used.)

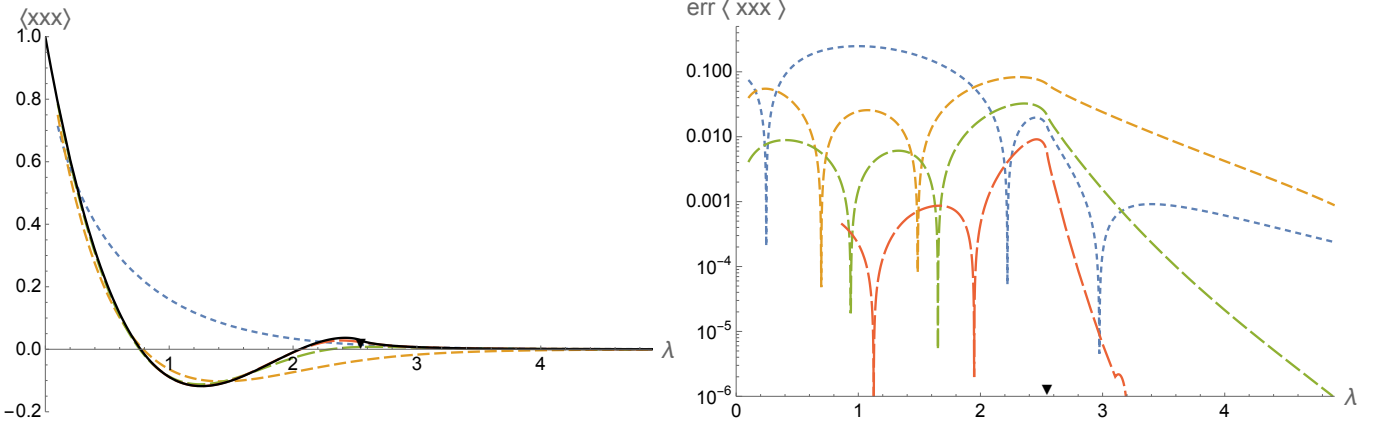


FIG. 6. Left: Triply winding loop expectation value $w_3 \equiv \langle xxx \rangle$ in the Hamiltonian one-plaquette model. Shown is the exact result (solid black line) and results from variational calculations using 1, 2, 4 and 8 generators. (The eight generator curve is only barely indistinguishable from the exact curve.) Right: Semi-log plot of the absolute error magnitude between exact and variational results with 1, 2, 4 and 8 generators. (The same line styles as in Fig. 4 are used.)

x -axis of these plots marks the position of the phase transition.

Just as in the Euclidean one-plaquette model, these results show good convergence as the number of generators increases. Unsurprisingly, the non-monotonic behavior of the triply-winding expectation w_3 requires more variational parameters to accurately reproduce.

Figure 7 shows a plot of the excitation energy to the first parity-even excited state, δE_1^+ , together with variational results using 2, 4 or 8 generators, while Fig. 8 shows a plot of the excitation energy to the first parity-odd excited state, δE_1^- , together with variational results using 2, 4 or 8 generators.

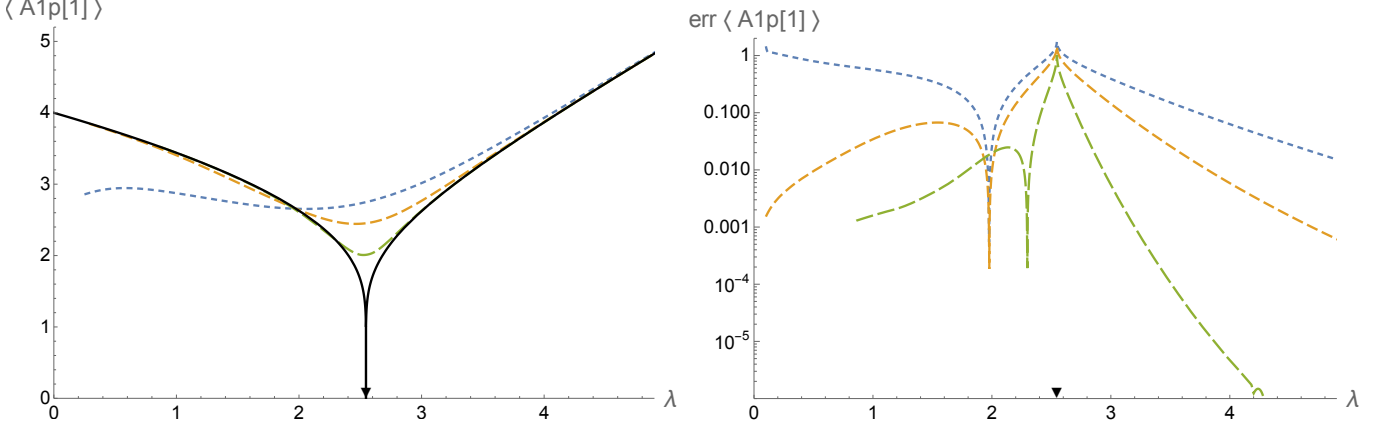


FIG. 7. Left: Excitation energy to the first parity-even excited state, δE_1^+ , in the Hamiltonian one-plaquette model. Shown is the exact result (solid black line) and results from variational calculations using 2, 4 and 8 generators. Right: Semi-log plot of the absolute error magnitude between exact and variational results with 2 (blue), 4 (orange) and 8 (green) generators; curves with progressively longer dashes have an increasing number of generators. The black triangle on the x -axis marks the position of the phase transition.

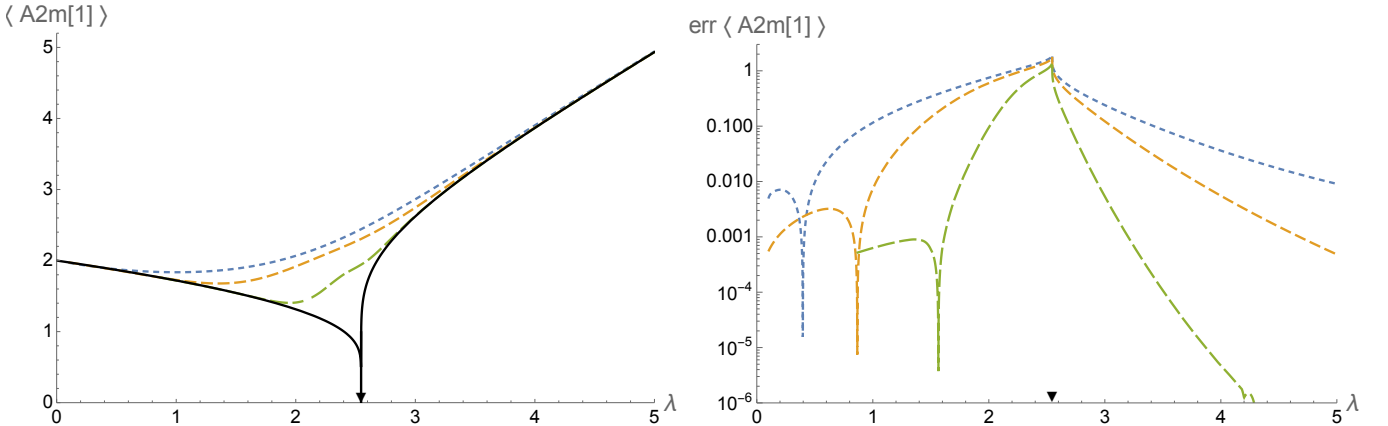


FIG. 8. Left: Excitation energy to the first parity-odd excited state, δE_1^- , in the Hamiltonian one-plaquette model. Shown is the exact result (solid black line) and results from variational calculations using 2, 4 and 8 generators. Right: Semi-log plot of the absolute error magnitude between exact and variational results with 2, 4 and 8 generators. (The same line styles as in Fig. 7 are used.)

The extremely abrupt vanishing of these excitation energies at the phase transition is unavoidably smoothed over by the variational results. Increasing numbers of variational parameters are needed to obtain results which do a better job of revealing the dramatic dip in the excitation energy around the transition.

C. 2D Euclidean Yang-Mills

As shown in Ref. [31], in two-dimensional Euclidean Yang-Mills theory on an infinite cubic lattice one may perform a change of variables from link variables to plaquette variables and, because there are no Bianchi identity constraints in two dimensions, each resulting plaquette variable is a completely independent group element. Consequently, the partition function reduces to an uncorrelated product of identical single plaquette integrals,

$$Z = \int \prod_{\ell} dU_{\ell} e^{-\frac{N}{\lambda} \sum_p \text{tr}(2 - U_{\partial p} - U_{\partial p}^{\dagger})} = \prod_{i,j} \int dP_{i,j} e^{-\frac{N}{\lambda} \text{tr}(2 - P_{i,j} - P_{i,j}^{\dagger})}. \quad (4.16)$$

Here $P_{i,j} \equiv U_{ij}^x U_{i+1,j}^y U_{i,j+1}^{x\dagger} U_{i,j}^{y\dagger}$ is the plaquette variable starting at lattice site (i,j) . The inverse relation is easiest to write in an axial gauge where all y -directed links are set to the identity, $U_{i,j}^y = 1$. Then (up to a y -independent gauge transformation):

$$U_{i,j}^x = \begin{cases} 1, & j = 0; \\ P_{i,j-1}^{\dagger} P_{i,j-2}^{\dagger} \cdots P_{i,0}^{\dagger}, & j > 0; \\ P_{i,j} P_{i,j+1} \cdots P_{i,-1}, & j < 0. \end{cases} \quad (4.17)$$

One can, of course, apply the coherent state variational algorithm to each of these independent one-plaquette models, in exactly the manner discussed above. But coherence group generators which act on a single plaquette while leaving all other plaquettes unchanged are, when expressed in terms of the original link variables and single link derivatives (or electric field operators), extremely non-local.²¹

A test of the coherent state variational method which is far more challenging than the previous applications to single plaquette models is to attempt to solve two-dimensional Euclidean Yang-Mills theory using coherence group generators of bounded extent *without* transforming to plaquette variables. This mimics what can be done in higher dimensional theories. An initial effort to do just this was made in Ref. [3], but with observable truncations which were more limited than what is possible to handle today.

Variational calculations were performed with generator truncations at order 2, 4 and 6, corresponding to one, two and three plaquette operators, and sets of observables truncated at strong-coupling orders up to 32. These are calculations with, respectively, 1, 4 and 13 variational parameters, and up to 115 million observables. Table II shows various statistics of the performed calculations, including the number of terms in the resulting sets of geodesic equations.

²¹ A “plaquette” generator $e_{i,j}^m$ satisfying $[e_{i,j}^m, P_{k,l}] = \delta_{i,k} \delta_{j,l} P_{i,j}^{1-m}$, when written in terms of the original link variables is an infinite sum. One may show that $e_{i,j}^m = \sum_{p=0}^{\infty} N \text{tr}[E_{i,j-p}^x (U^y)^p (U^y U^x U^y \dagger U^x \dagger)^m (U^y)^{-p}]$ is a valid form. (The site indices of the link variables are suppressed, but are uniquely determined by the requirement that the operator be a sensible closed loop.)

generator order limit	observable order limit	# variational parameters	total # observables	# geodesic terms	info file size
2	16	1	219	—	— ^a
2	20	1	4,208	—	— ^a
2	24	1	113,662	—	— ^a
2	28	1	3,493,718	—	— ^a
4	16	4	219	3.4×10^3	116 KB
4	20	4	4,208	9.8×10^4	1.98 MB
4	24	4	113,662	3.3×10^6	62.6 MB
4	28	4	3,493,718	1.2×10^8	2.22 GB
4	32	4	115,452,663	4.5×10^9	80.6 GB
6	20	13	4,208	2.5×10^5	6.91 MB
6	24	13	113,662	8.1×10^6	158 MB
6	28	13	3,493,718	2.9×10^8	4.7 GB
6	32	13	115,452,663	1.1×10^{10}	175 GB

^a These calculations used order 4 system information files with forth order generators turned off during minimization.

TABLE II. Statistics of variational calculations performed in two-dimensional Euclidean Yang-Mills theory. The penultimate column gives the total number of terms in the complete set of geodesic equations for the given calculation, while the final column gives the size of the system information file which records the selected sets of observables and generators, and the resulting expressions for the free energy gradient, curvature, and geodesic equations.

Figure 9 shows the results for the free energy obtained from variational calculations with order 2, 4 and 6 generators and observable truncation at order 28. In the left-hand plot of the free energy, the green order 6 curve (with longest dashes) is barely distinguishable from the exact result.

The subsequent figures 10–13 show, respectively, the corresponding results for the expectation values of a single plaquette, a 2×1 rectangular loop, a 2×1 figure eight loop, and a winding two plaquette. The exact answer for both rectangular and figure eight 2×1 loops is just the square of the single plaquette expectation value.

From these plots, it is apparent that the coherent state variational algorithm, with a modest number of variational parameters, is working quite well down to values of the gauge coupling well into the weak coupling regime.

Figures 14 illustrate the dependence on the observable truncation order. Shown are results for expectation values of the elementary plaquette, 2×1 rectangular and figure eight loops and the winding two plaquette, from variational calculations with order 4 generators and observable truncations at order 20, 24 and 28. It is evident that, for these calculations, the observable truncation effects are quite small when $\lambda \gtrsim 1$ but start becoming larger around $\lambda \approx 0.7$. With the same set of observable truncations and order 6 generators, calculations show somewhat larger observable truncation effects, as one would expect, with

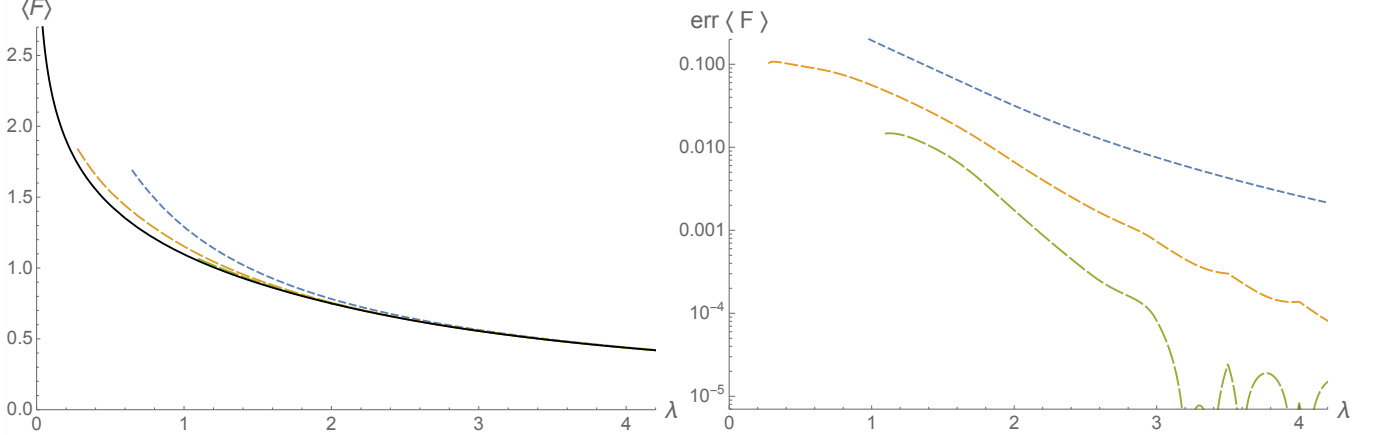


FIG. 9. Left: Free energy of two-dimensional Euclidean Yang-Mill theory. Shown is the exact result (solid black line) and results from variational calculations using order 2, 4 and 6 generators and observable truncation at order 28. Right: Semi-log plot of the absolute error magnitude between exact and variational results with order 2, 4 and 6 generators. (Line styles are the same as in earlier figures.)

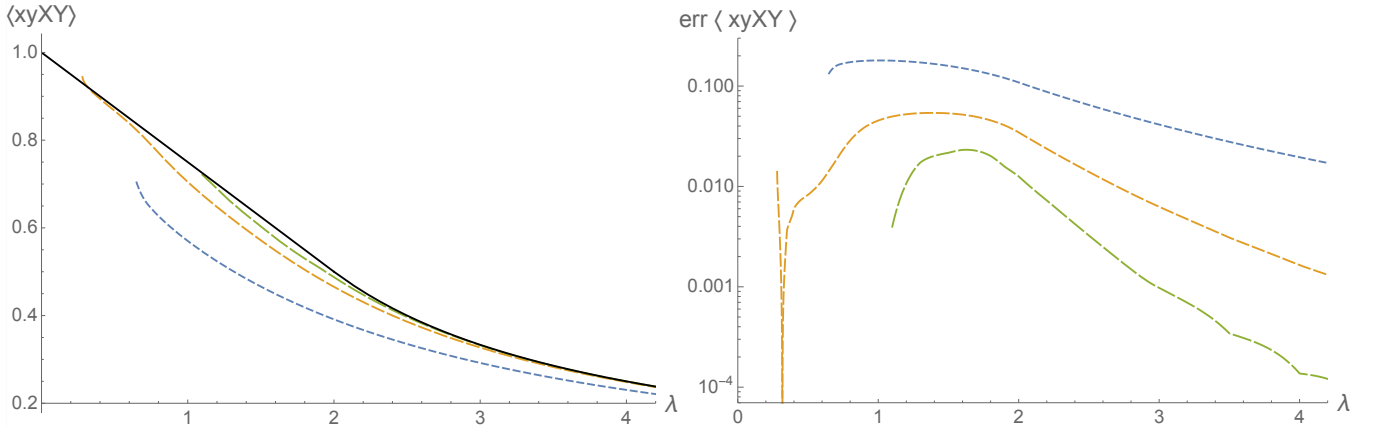


FIG. 10. Left: Expectation value of the single plaquette $\langle xyXY \rangle$ in two-dimensional Euclidean Yang-Mill theory. Shown is the exact result (solid black line) and results from variational calculations using order 2, 4 and 6 generators and observable truncation at order 28. Right: Semi-log plot of the absolute error magnitude between exact and variational results with order 2, 4 and 6 generators. (Line styles as in earlier figures.)

good agreement between the different truncations down to $\lambda \approx 1.5$ and more noticeable divergence below $\lambda \approx 1.2$.

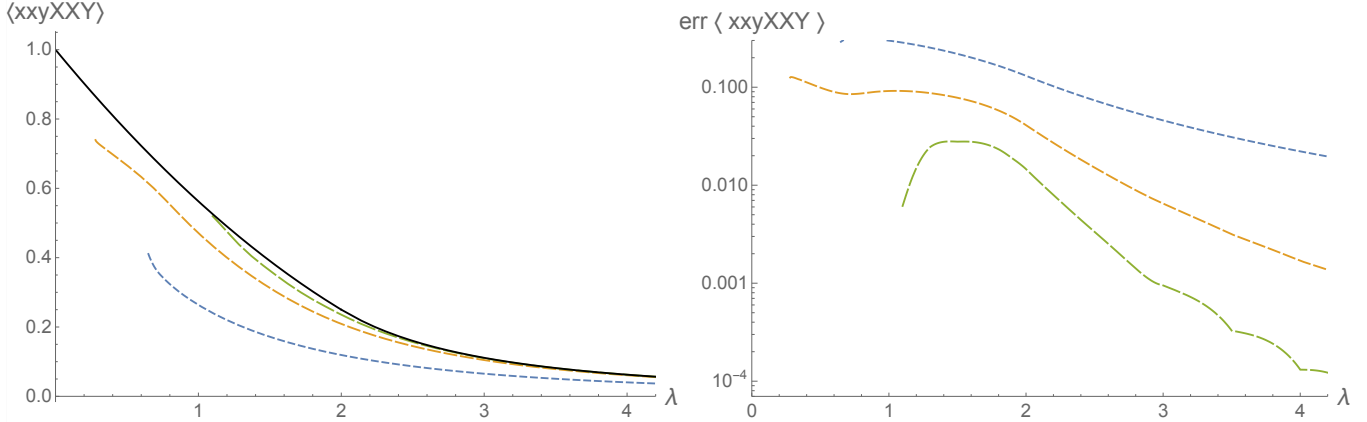


FIG. 11. Left: Expectation value of the 2×1 rectangular loop $\langle xxyXXY \rangle$ in two-dimensional Euclidean Yang-Mill theory. Shown is the exact result (solid black line) and results from variational calculations using order 2, 4 and 6 generators and observable truncation at order 28. Right: Semi-log plot of the absolute error magnitude between exact and variational results with order 2, 4 and 6 generators. (Line styles as in earlier figures.)

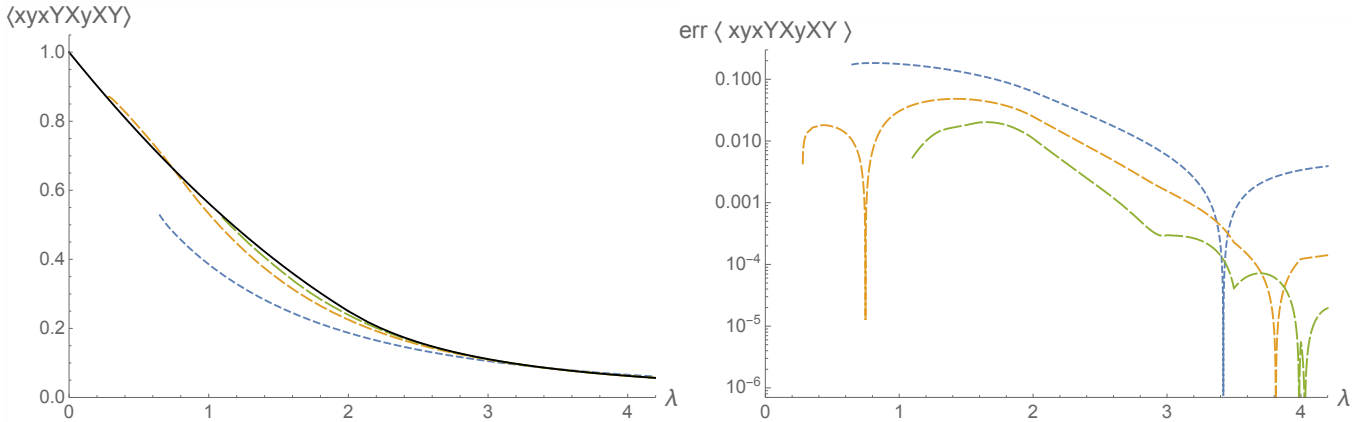


FIG. 12. Left: Expectation value of the two plaquette figure eight loop $\langle xxyXXyXY \rangle$ in two-dimensional Euclidean Yang-Mills theory. Shown is the exact result (solid black line) and results from variational calculations using order 2, 4 and 6 generators and observable truncation at order 28. Right: Semi-log plot of the absolute error magnitude between exact and variational results with order 2, 4 and 6 generators. (Line styles as in earlier figures.)

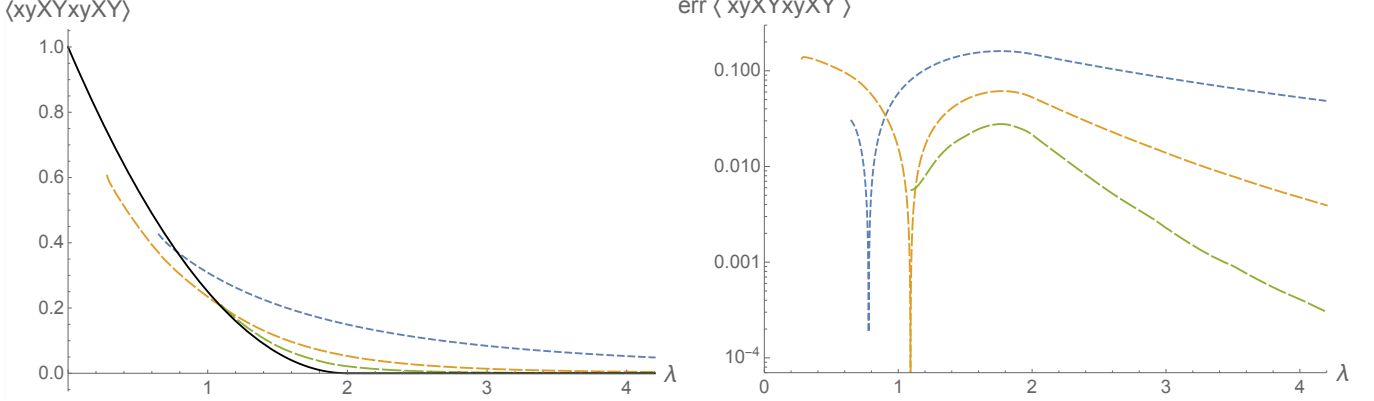


FIG. 13. Left: Expectation value of the winding two plaquette $\langle xyXYxyXY \rangle$ in two-dimensional Euclidean Yang-Mill theory. Shown is the exact result (solid black line) and results from variational calculations using order 2, 4 and 6 generators and observable truncation at order 28. Right: Semi-log plot of the absolute error magnitude between exact and variational results with order 2, 4 and 6 generators. (Line styles as in earlier figures.)

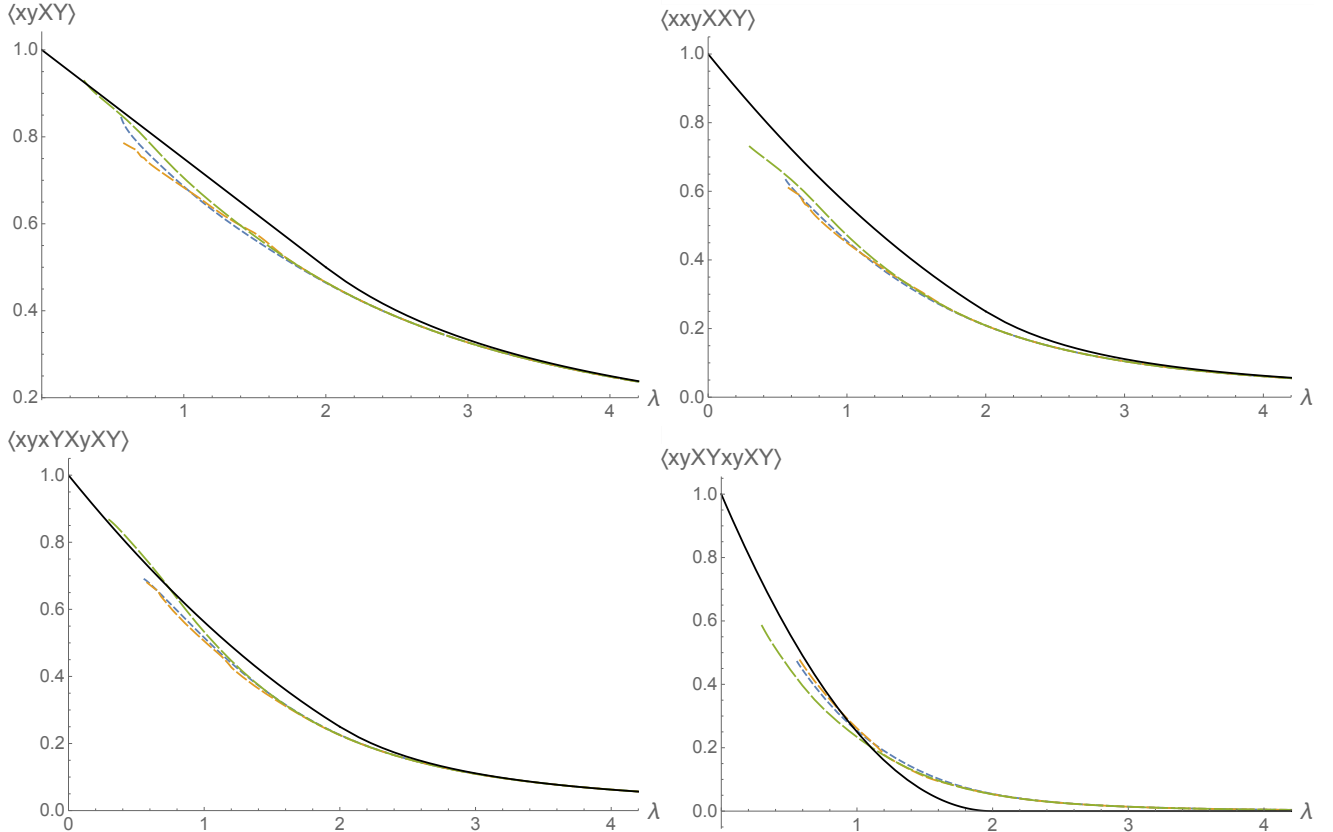


FIG. 14. Illustration of observable truncation effects: comparisons of results for expectation values of the indicated loops using order 4 generators and observable truncations at order 20, 24 and 28. (Line styles as in earlier figures.)

generator order limit	observable order limit	# variational parameters	total # observables	# geodesic terms	info file size
2	16	1	22,987	—	— ^a
2	20	1	991,145	—	— ^a
2	24	1	44,328,221	—	— ^a
4	16	4	22,987	2.0×10^6	48.9 MB
4	20	4	991,145	1.2×10^8	2.83 GB
4	24	4	44,328,221	6.3×10^9	154 GB
6	16	13	22,987	9.5×10^6	241 MB
6	20	13	991,145	6.4×10^8	15.6 GB
6	24	13	44,328,221	3.9×10^{10}	937 GB

^a These calculations used order 4 system information files with forth order generators turned off during minimization.

TABLE III. Statistics of variational calculations performed in 2+1 dimensional Hamiltonian Yang-Mills theory. The penultimate column gives the total number of terms in the complete set of geodesic equations for the given calculation, while the final column gives the size of the system information file which records the selected sets of observables and generators, and the resulting expressions for the Hamiltonian gradient, curvature, and geodesic equations.

D. 2+1D Hamiltonian Yang-Mills

The 2+1 dimensional Yang-Mills Hamiltonian is given by Eq. (2.5), with an infinite two-dimensional cubic lattice. Symmetry representations which will classify zero-momentum excited states, and onto which coherence algebra generators will be projected, are given by irreducible representations of the C_{4v} crystallographic group, conventionally named A_1 , A_2 , B_1 , B_2 and E , augmented by a \pm superscript (or a p or m suffix in plots) indicating the sign change of the representation under charge conjugation.

Variational calculations were performed with generator truncations at order 2, 4 and 6, corresponding to one, two and three plaquette operators, and sets of observables truncated at strong-coupling orders up to 24. These are calculations with, respectively, 1, 4 and 13 variational parameters, and up to 44 million observables. Table III shows various statistics of the performed calculations, including the number of terms in the resulting sets of geodesic equations.

Figure 15 shows the results for the ground state energy and the expectation values of a single plaquette, a 2×1 loop, and a winding-two plaquette obtained from variational calculations with order 2, 4 and 6 generators and observable truncation at order 24.

The following figure 16 shows results for the lowest glueball mass in the A_2^- and A_1^+ symmetry channels, using order 2, 4 and 6 generators and observables truncated at strong-coupling order 24. The A_2^- glueball is the lightest excitation, followed by the A_1^+ glueball. These glueball masses asymptote to 4λ at strong coupling.

The subsequent figure 17 shows results for the lowest glueball mass in the B_1^+ , B_2^- and

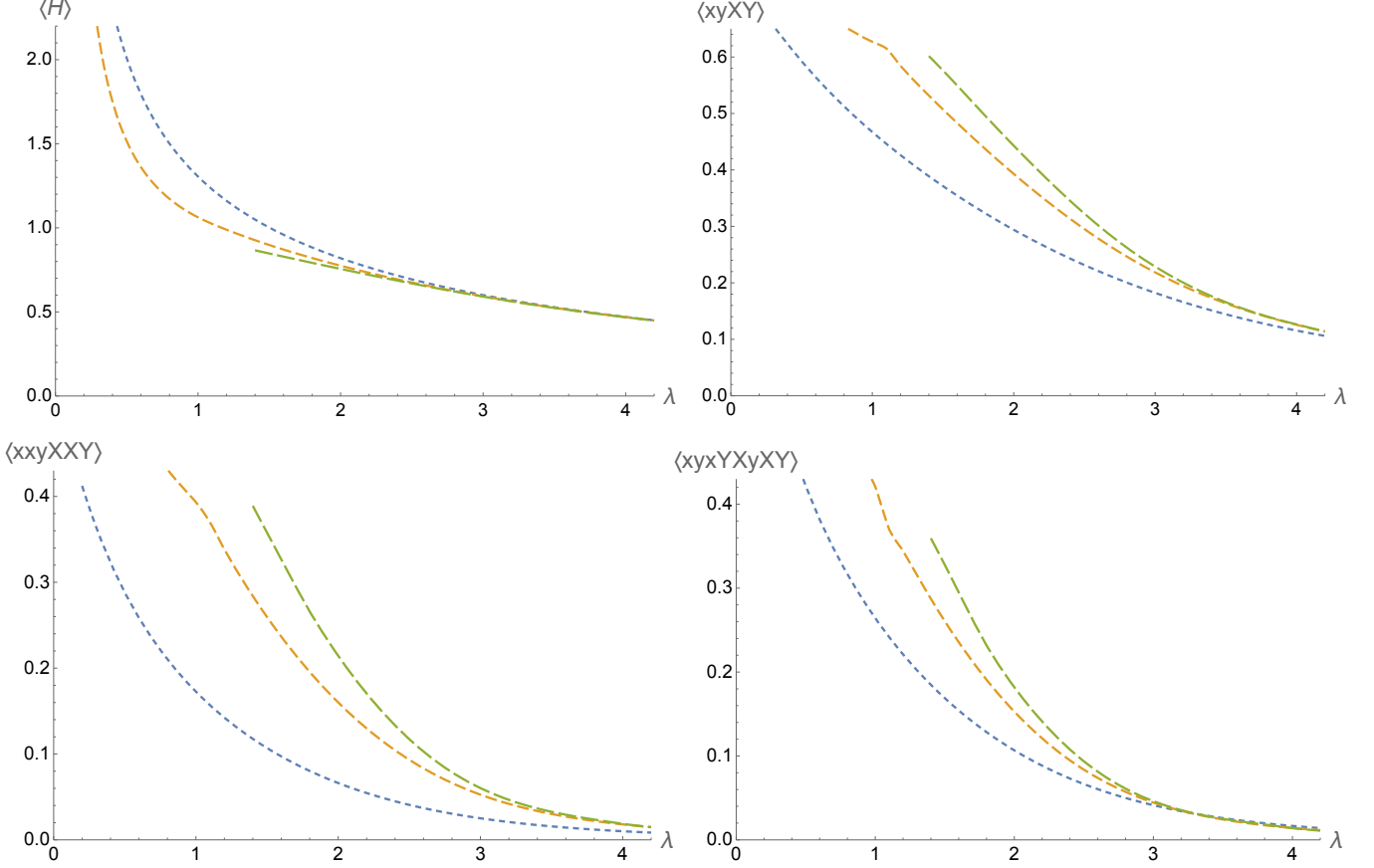


FIG. 15. Ground state energy (upper left) and expectation values of a single plaquette $\langle xyXY \rangle$ (upper right), 2×1 loop $\langle xxyXXY \rangle$ (lower left), and winding-two plaquette $\langle xyXYxyXY \rangle$ (lower right) in 2+1 dimensional Hamiltonian Yang-Mills theory. Shown are results from from variational calculations using order 2, 4 and 6 generators and observable truncation at order 24. (Line styles are the same as in earlier figures, with longer dashed curves corresponding to higher order truncations.)

E^- symmetry channels obtained from variational calculations with 4 and 6 generators and observable truncation at order 24. Order 2, or single plaquette, generators do not project onto these representations. The B_1^+ and B_2^- glueball masses asymptote to 6λ at strong coupling, while the E^- glueball asymptotes to 8λ .

The final figure 18 in this subsection shows results for the lowest glueball mass in each of the remaining symmetry channels: B_2^+ , B_1^- , E^+ , A_1^- and A_2^+ . The results shown come from variational calculations with order 6 generators and observable truncation at order 24. The lowest order for which a generator can project onto any of these representations is order 6. In the figure, the lowest, shortest dash line (for $\lambda \gtrsim 1.5$) is the B_2^+ curve, while the progressively increasing curves show the results for representations B_1^- , E^+ , A_1^- and A_2^+ , in that order.

Discussion of these results is postponed to section VI.

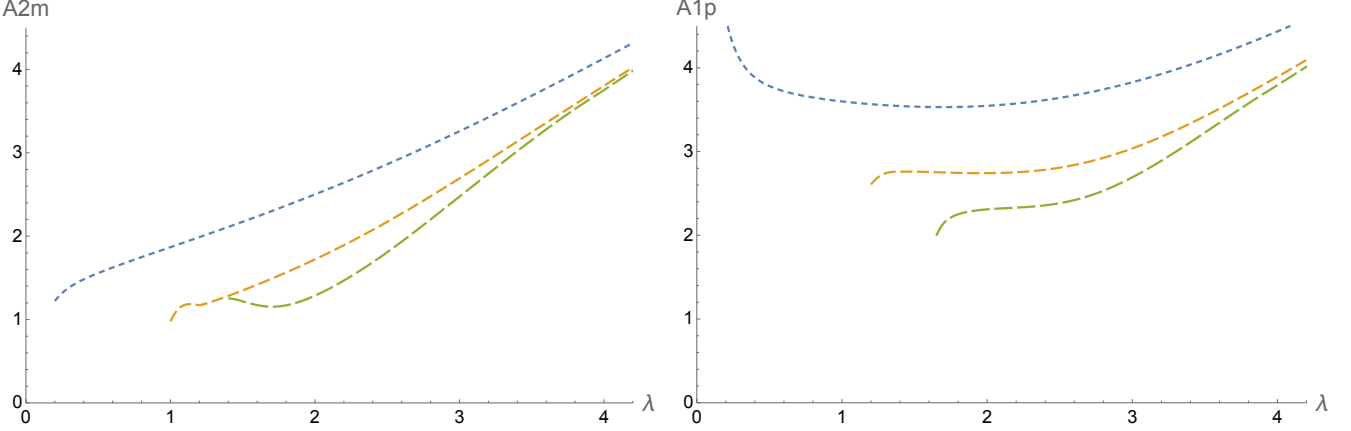


FIG. 16. Results for the lowest glueball mass in the A_2^- and A_1^+ symmetry channels from variational calculations using order 2, 4 and 6 generators and observable truncation at order 24. (Line styles as in earlier figures.)

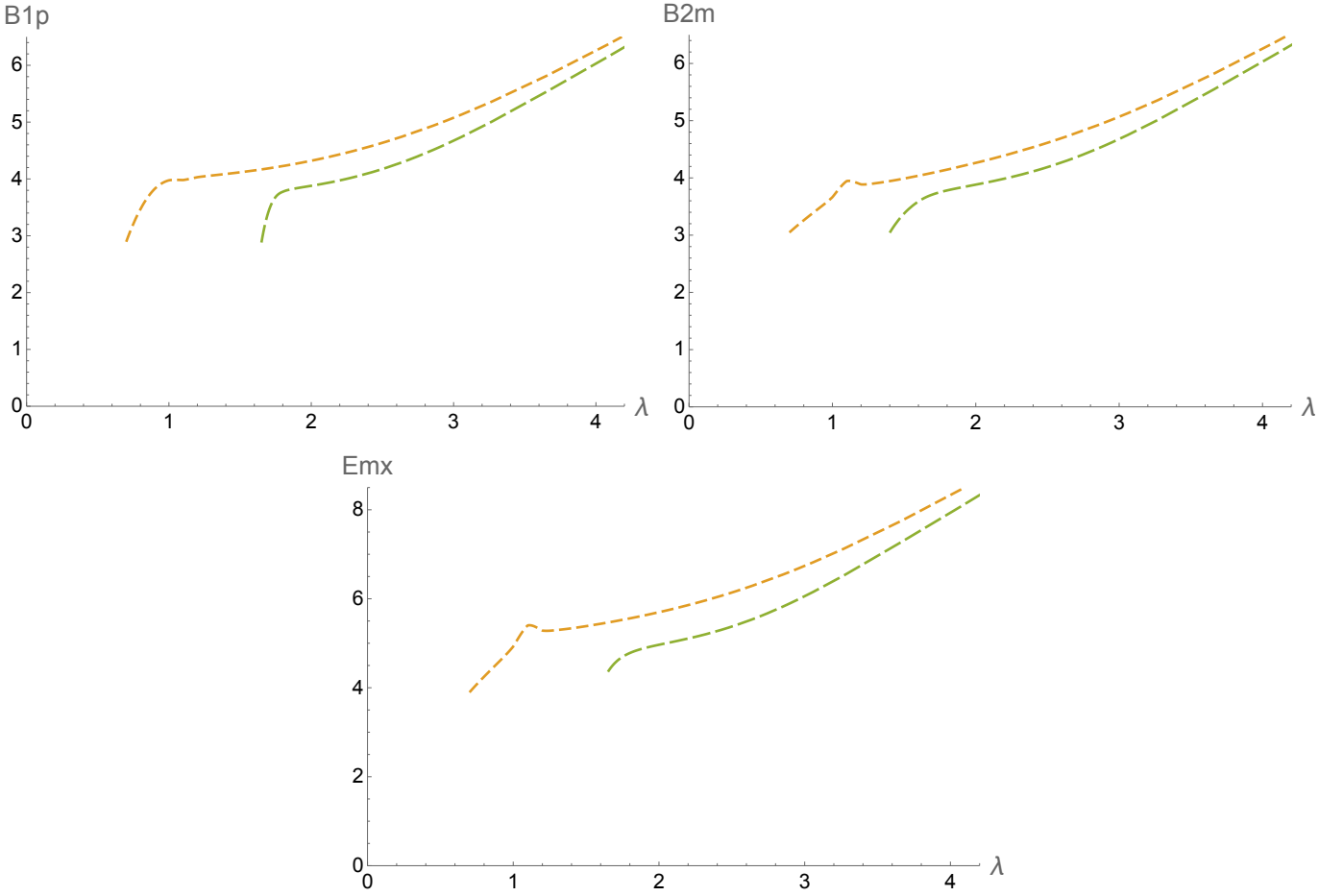


FIG. 17. Results for the lowest glueball mass in the B_1^+ , B_2^- and E^- symmetry channels from variational calculations using order 4 and 6 generators and observable truncation at order 24. (Line styles as in earlier figures.) Note that order 2 (single plaquette) generators cannot project onto these representations.

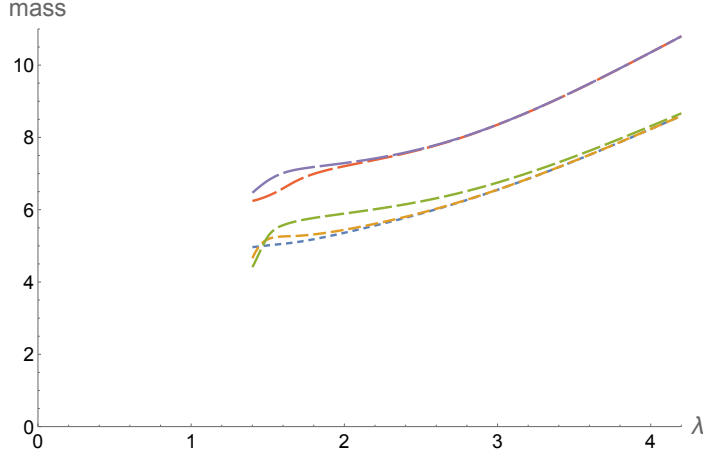


FIG. 18. Results for the lowest glueball mass in the B_2^+ (shortest dash, blue), B_1^- (orange), E^+ (green), A_1^- (red) and A_2^+ (longest dash, purple) representations from variational calculations using order 6 generators and observable truncation at order 24. Note that order 6 is the minimal order for which generators can project onto these representations.,

V. OBSERVABLE APPROXIMATION

In the results presented above, as well as prior work exploring applications of the coherent state variational algorithm [2, 3, 27–29], any term in a geodesic equation or curvature matrix element involving an observable *not* in the retained set was simply dropped. In other words, the expectation values of all non-retained observables were approximated by zero. With observable selection based on the strong-coupling order classification, this provides a good approximation at least for some range of sufficiently strong coupling. Inevitably, however, for any given truncation of the set of observables, errors in the state representation caused by this truncation will grow as the lattice gauge coupling is decreased and the ground state correlation length grows.

A natural question to consider is whether it is possible to do a better approximation for the expectation values of observables outside the truncation set. Can the expectation values of non-retained observables be usefully approximated by some simple functions of the expectation values of retained observables? This idea is motivated by the observation that nearly all Wilson loops are self-intersecting (with the small fraction of non-self intersecting loops dropping rapidly with increasing strong-coupling order). From studies of confinement, it is known that expectation values of simple, planar non-self intersecting Wilson loops are well-described by a combination of area-law and perimeter-law behavior at both strong and weak coupling,

$$W_\Gamma \approx e^{-\gamma|\Gamma| - \sigma \text{area}(\Gamma)}, \quad (5.1)$$

where $|\Gamma|$ is the perimeter of a loop Γ , $\text{area}(\Gamma)$ is the minimal area of a surface spanning Γ , σ is the string tension and γ is a (UV sensitive) perimeter-law coefficient. To the extent that such a combination of area-law and perimeter-law terms provides a good approximation for most Wilson loops — which is a major untested assumption — then the expectation value

generator order limit	observable order limit	geodesic terms		info file size	
		w/o approx	with approx	w/o approx	with approx
4	16	3.4×10^3	2.3×10^4	116 KB	433 KB
4	20	9.8×10^4	9.5×10^5	1.98 MB	15.6 MB
4	24	3.3×10^6	4.1×10^7	62.6 MB	659 MB
4	28	1.2×10^8	1.7×10^9	2.22 GB	28.1 GB
6	20	2.5×10^5	7.9×10^6	6.91 MB	132 MB
6	24	8.1×10^6	3.7×10^8	158 MB	5.98 GB
6	28	2.9×10^8	1.7×10^{10}	5.07 GB	270 GB

TABLE IV. 2D Euclidean Yang-Mills: Comparisons of the number of geodesic equation terms, and resulting system information file sizes, with and without approximation of non-retained observables, for varying orders of generator and observable truncation.

of a self-intersecting loop which is the composition of two (individually closed) sub-loops, $\Gamma = \Gamma_1 \Gamma_2$, should approximately satisfy the factorization relation

$$W_\Gamma \approx W_{\Gamma_1} \times W_{\Gamma_2}, \quad (5.2)$$

since the sum of the sub-loop perimeters equals the whole loop perimeter, and the composition of the sub-loop spanning surfaces is a spanning surface of the whole loop.²²

For any geodesic equation term involving a loop Γ which is not in the retained set of observables, if that loop can be factored into sub-loops which are found in the retained set then approximating the expectation value W_Γ as a product of sub-loop expectations may reduce the truncation error in the state representation. This, it must be emphasized, is merely a hypothesis, but one which seems worth exploring.

The current *Gordion* code optionally implements such an observable approximation scheme. The relevant routine examines all self-intersections of an observable appearing in a commutator result which is found to be outside the truncation set. Each self-intersection is assigned a numeric score which is used to select preferred possible factorizations when there are multiple possibilities. The particulars of this intersection scoring are chosen to favor factorizations which split the observable into comparably-sized pieces, as this should maximize the probability that both sub-observables do lie within the truncation set. Factorization is attempted not just for Wilson loops, but also for Wilson loops containing electric field insertions (as well as fermion bilinears). The precise details of this scoring and factorization algorithm are unquestionably rather ad-hoc and are described more fully in Ref. [30].

One unavoidable consequence of applying this observable approximation scheme is a major increase in the number of terms in the resulting geodesic equations, and consequent storage requirements, as detailed in Tables IV and V.

²² In 2D Euclidean Yang-Mills, this relation is exact for self-intersecting loops whose minimal spanning surfaces are disjoint and unfolded. More generally, however, there are cases where the sum of the sub-loop areas does not equal the *minimal* area of a spanning surface of the full loop.

generator order limit	observable order limit	geodesic terms		info file size	
		w/o approx	with approx	w/o approx	with approx
4	16	2.0×10^6	9.7×10^6	48.9 MB	233 MB
4	20	1.2×10^8	6.3×10^8	2.83 GB	15.3 GB

TABLE V. 2+1D Hamiltonian Yang-Mills: Comparisons of the number of geodesic equation terms, and resulting system information file sizes, with and without observable approximation of non-retained observables, for order 4 generator and observable truncation at order 16 or 20.

Some results of this initial effort at observable approximation are shown in Figs. 19 and 20. Figure 19 compares deviations from the exact results in 2D Euclidean Yang-Mills for the winding-1 plaquette expectation value $\langle xyXY \rangle$ and the winding-2 plaquette expectation $\langle xyXYxyXY \rangle$ from variational calculations with order 4 generators and observable truncation, with and without observable approximation, at orders 20 and 24. Figure 20 compares results in 2+1D Hamiltonian Yang-Mills for the lowest A_2^- and A_1^+ glueball masses from variational calculations with order 4 generators and observable truncation, with and without observable approximation, at orders 16 and 20, and without observable approximation at order 24.

These results are less promising than hoped for. The most salient feature is the lack of any clear conclusion regarding the utility of this simplest observable approximation scheme. In the 2D Euclidean results, the order 20 curves for $\langle xyXY \rangle$ with observable approximation (orange curve of the left panel of Fig. 19) do not have smaller deviations from the exact result, or from the order 24 curves, than do the unapproximated order 20 results (blue curve). The order 24 results for $\langle xyXY \rangle$ with observable approximation (red curve) deviates more from the exact result than does the unapproximated order 24 curve (green). However, this comparison flips for the $\langle xyXYxyXY \rangle$ results shown on the right panel of Fig. 19: the observable approximation result is somewhat more accurate than the unapproximated result. Results for other observables, comparing order 24 observable truncations with and without observable approximation are similarly variable, with the observable approximation results sometimes better and sometimes worse.

In the 2+1D Hamiltonian Yang-Mills results shown in Fig. 20, the most salient feature is again the lack of any clear conclusion regarding the effect of this simplest observable approximation scheme. In results for the ground state energy, or for expectations of small loops such as $\langle xyXY \rangle$, $\langle xxyXXY \rangle$, or $\langle xyXYxyXY \rangle$, the dependence on the observable truncation order is quite small and the effect of using observable approximation for non-retained observables is nearly imperceptible in plots of these observables. The same is true for the lowest A_2^- glueball mass, shown on the left of Fig. 20. But results for the lowest A_1^+ glueball mass, shown on the right of Fig. 20, display much larger dependence on the observable truncation order, with a negligible difference between the order 16 results with and without observable approximation, and only rather small difference between the order 20 results with and without such approximation above $\lambda \approx 0.7$. In the A_1^+ mass results (as well as most other symmetry channels) the results using observable approximation at one given truncation order cannot be said to nearly mimic unapproximated results at a higher observable truncation order.

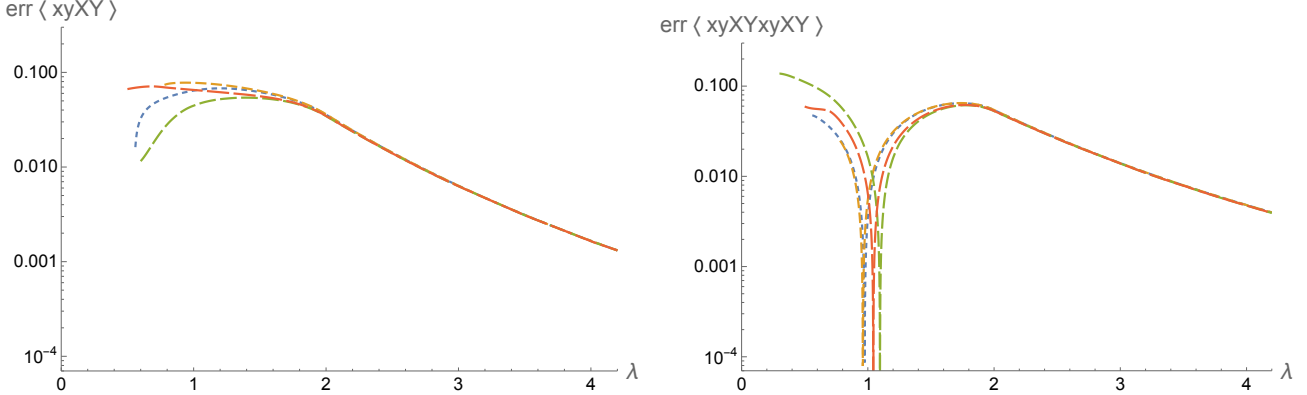


FIG. 19. Comparisons, in 2D Euclidean Yang-Mills, of the deviation from the exact results when observable approximation is, or is not, employed. Shown are the deviations from exact results for the single plaquette expectation $\langle xyXY \rangle$ (left panel) and the double winding plaquette expectation $\langle xyXYxyXY \rangle$ (right panel) from variational calculations with order 4 generators and observable truncation at orders 20 and 24. Blue (shortest dash) and orange curves (next shortest dash) are order 20 observable truncation results, without and with observable approximation, respectively. Green and red (longest dash) curves are order 24 observable truncation results, without and with observable approximation, respectively.

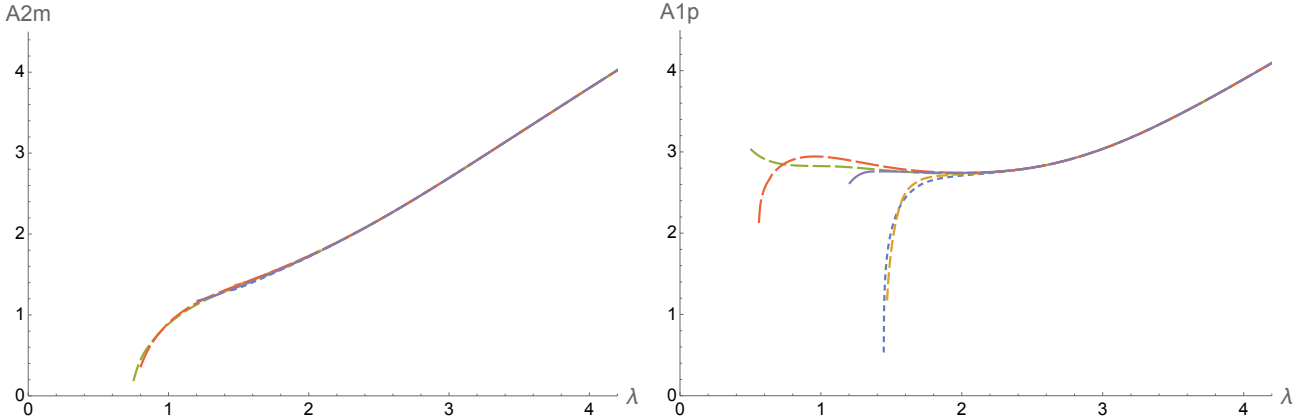


FIG. 20. Comparisons, in 2+1D Hamiltonian Yang-Mills, of results when observable approximation is, or is not, employed. Shown are results for the lowest A_2^- and A_1^+ glueball masses from variational calculations with order 4 generators and observable truncation at orders 16, 20 and 24. Blue (shortest dash) and orange curves are for order 16 observable truncation, without and with observable approximation, respectively, while green and red (progressively longer dashes) curves are for order 20 observable truncation, without and with observable approximation, respectively, and purple (longest dash) shows observable 24 results without observable approximation.

Possibilities for improving this initial observable approximation scheme are briefly discussed in the conclusions.

VI. DISCUSSION

The various results presented in section IV illustrate both the potential and the challenges involved in applying the coherent state variational algorithm to large N gauge theories. The results for single plaquette models, both Euclidean and Hamiltonian, in sections IV A and IV B attest both to the correct functioning of the *Gordion* code and to the feasibility of obtaining good results from this variational approach in theories having continuous phase transitions. The results on two dimensional Euclidean Yang-Mills theory in section IV C show, completely unsurprisingly, that without using the non-local reduction to independent plaquette variables much larger observable truncation sets are needed to obtain good results. Nevertheless, the results of section IV C show that this is quite feasible today.

The results for 2+1D Hamiltonian Yang-Mills theory in section IV D reveal how much more demanding the Hamiltonian theory on a two-dimensional spatial lattice is in comparison to the Euclidean theory on the same lattice. In part, this reflects the much larger size of observable sets (of a given truncation order) in Hamiltonian theories due to the need to include Wilson loops with two electric field insertions. But the plots of section IV D also show notably slower convergence of results with increasing order of the generator selection (or number of variational parameters) as compared to the analogous 2D Euclidean results.

In 2+1D lattice Yang-Mills theory, if one inserts a lattice spacing a to define the (inverse) cutoff scale, then the dimensionless lattice coupling $\lambda = a g^2 N$, with the 't Hooft coupling $g^2 N$ having dimensions of mass. In the lattice regulated theory each glueball mass, in units of a^{-1} , is some function of the lattice coupling, $m a = f(\lambda)$. In the continuum limit, each such glueball mass must be some pure number c times $g^2 N$, as there is no other relevant scale, and hence lattice glueball masses, times a , must have the weak coupling form $f(\lambda) = c \lambda + O(\lambda^2)$ as $\lambda \rightarrow 0$. Or in other words, lattice glueball masses must approach a straight line through the origin. Similarly, every Wilson loop expectation value, for any fixed lattice loop Γ , must approach a straight line with intercept one, $\langle W_\Gamma \rangle = 1 + c_\Gamma \lambda + O(\lambda^2)$.

The results reported in section IV D reach values of λ at which the single plaquette Wilson loop expectation value exceeds 0.5, and the order 6 curves for the small loop expectation values shown in Fig. 15 are certainly consistent with a very smooth linear approach to 1 as $\lambda \rightarrow 0$ with small higher order corrections. But the analogous statement cannot be made for the various glueball mass curves plotted in figures 16–18. The highest (sixth) order curves plotted in these figures do not yet convincingly show linear approach to the origin.

Despite the truncation-induced limitations in the current results for glueball masses in 2+1D Yang-Mills, one might nevertheless attempt to extract an estimate (or crude best guess) for the continuum limit of light glueball masses by drawing straight lines from the origin which intersect with the order 6 curves in figures 16–18 at a point of tangency. Regarding this as providing a serious estimate of continuum masses is, of course, clearly premature. First, the significant changes seen in Figs. 16 and 17 between the results of fourth and sixth order generator truncations (or 4 to 13 variational parameters) strongly suggests that inclusion of yet higher order generators will be needed before decently converged results can be obtained. Second, in the continuum limit the B_1^+ and B_2^+ masses should become degenerate

as these are both components of a spin-2 continuum representation, and likewise for B_1^- and B_2^- masses. The plotted results do not yet show any such near degeneracy between these channels.²³

Results from any given variational calculation will cease to provide a good approximation when the effects of the truncation in the selected sets of either observables or generators become undesirably large, and it is inevitable that such truncation effects will grow with decreasing coupling (or increasing correlation length). The location, and manner, of the resulting breakdown varies with the particular truncations employed. This is reflected in the varying termination points of plotted results in the various figures in section IV. Truncation induced problems can manifest in different ways as the coupling is lowered:

1. The curvature matrix (2.15) may cease to have purely real and positive eigenvalues, with either some eigenvalue going negative, or else complex conjugate pairs of eigenvalues appearing.
2. Certain Wilson loop expectations can move into the unphysical domain and, in particular, develop magnitudes exceeding unity.
3. The results may lack obvious internal inconsistencies but simply differ substantially from higher order calculations.

Complex curvature eigenvalues can appear because the coherence generator induced variations defining the curvature matrix are not coordinate derivatives and amount to using a non-coordinate set of basis vectors at any point in the large N phase space. Consequently, the curvature matrix (2.15) is not exactly symmetric. By the Jacobi identity, the antisymmetric part of the curvature matrix equals the gradient of the Hamiltonian in the direction of a commutator of generators, $(d^2H)_{[ij]} = \langle [[H, [e_i, e_j]]] \rangle$. Because only a finite set of generators can be retained, this commutator of generators may lie outside the set of selected generators. The size of this antisymmetric part is negligible at strong coupling, but grows as the coupling decreases. At some point this can cause pairs of curvature eigenvalues which are initially real to collide and move off into the complex plane. This may indicate that the generator truncation is no longer sufficient to obtain good results at a given value of coupling.

In Hamiltonian theories, the curvature matrix d^2H (2.15) is block diagonal with one block involving double commutators with pairs of time-reversal even generators and one block involving double commutators with pairs of time-reversal odd commutators,²⁴ while

²³ However, if one does boldly extrapolate by drawing a tangent through the origin to the order 6 curves, one finds $m/g^2N \approx 0.9$ for the lightest A_1^+ glueball, reasonably close to the value of 0.81 obtained in Ref. [11] from Euclidean lattice simulations. Results for other representations differ more substantially, with $m/g^2N \approx 0.65$ for the lightest A_2^- glueball, well below the value of 1.2 from Ref. [11], while for other channels the crudely extrapolated slopes are well above the Euclidean simulation values.

²⁴ For a detailed discussion of lattice symmetries and their implications for coherence group generators and observables, see appendix C of the implementation notes [30].

the Lagrange bracket matrix (2.16) is block odd-diagonal, with the non-vanishing components involving a commutator of a T -even generator with a T -odd generator.

The iterative minimization (in Hamiltonian theories) is only sensitive to the T -even block of the curvature matrix in the completely symmetric lattice symmetry channel, since the gradient in time-reversal odd directions automatically vanishes. For Newton minimization to show the expected quadratic convergence, it is essential that non-symmetric definition (2.15) of the curvature be used when predicting the location of the minimum.

The small oscillation eigensystem (2.18), in any given symmetry channel, depends on both the T -even and T -odd blocks of the curvature as well as the Lagrange bracket matrix L . The curvature matrix may be symmetrized for spectrum calculations, guaranteeing purely real symmetrized curvature eigenvalues. If both blocks of the curvature are positive definite then the small oscillation eigensystem (2.18) necessarily yields real oscillation frequencies (in \pm pairs). But if either block of the curvature matrix develops a negative eigenmode, then complex oscillation frequencies may appear in the computed small oscillation spectrum. Should this occur, this is a clear sign that one is beyond the regime of utility of a given truncation for the particular symmetry channel. For example, in the order 4 spectrum results for the A_1^+ , A_2^- and B_1^+ channels, shown as the orange curves in Figs. 16 and 17, negative curvature eigenvalues develop around couplings of 1.2, 0.9 and 0.6, respectively, leading to the lowest oscillation frequencies in these channels becoming unphysical.

For some truncations, a complex or negative curvature eigenvalue which eventually appears may correspond to a variational direction in which the gradient of the Hamiltonian (or free energy) is very small, so that the presence of this non-positive eigenvalue below some value of coupling may have very little impact on the iterative Newton extremization (even though it indicates that the truncation is not well describing some variation which is nearly transverse to the gradient). But eigenvalues which are highly sensitive to the truncation and, at some value of coupling, pass through zero can lead to completely invalid predictions (2.17) for the location of an extremum and consequent complete failure of convergence of the Newton iterative extremization. This failure mode can sometimes (but not always) be tamed by using a singular value pseudoinverse, i.e., performing a singular value decomposition of the curvature and omitting contributions to the inverse curvature coming from singular values whose magnitude falls below a chosen cutoff. In, for example, the order 6 generator, order 28 observable results for 2D Euclidean Yang-Mills, appearing in Figs. 9–13, a singular value cutoff of 0.6 was used below $\lambda = 2$. No sign of the imposition of this singular value cutoff at $\lambda = 2$ is visually apparent in the generator order 6 curves in these figures. But quite often an eigenvalue going negative (in the T -even block of the symmetric lattice symmetry channel) does signal the end of utility of a given calculation.

For a given set of generators, if the observable truncation order is sufficiently low then the resulting expressions for curvature matrix elements may have expectation values either omitted or approximated for observables which should have appeared but are above the truncation limit. This can lead to negative or complex curvature eigenvalues appearing even at rather large values of coupling. For example, in 2+1D Yang-Mills, if one attempts to use order 6 generators with observable truncation at order 16, a negative curvature eigenvalue

appears already at $\lambda \approx 2.15$. Consequently, calculations with order k observables should generally retain at least up to order $4k$ observables. Given the rapid growth in the size of observable sets, and storage needed for the geodesic equations, this concern is the major issue which prevented going to generator orders above 6 in the presented 2+1D Hamiltonian Yang-Mills calculations.

With a loop-list observable truncation scheme, a separate issue is that the geodesic equations for observables of highest order within the retained set are necessarily “damaged” by the omission (or imperfect approximation) of observables of yet higher orders. Consequently, integrating the finite, truncated set of geodesic equations can, at some point, lead to unphysical expectation values of Wilson loops which, for example, violate the basic unitarity bound $|W_\Gamma| \leq 1$. The good news, so to speak, is that such unitarity violations in high order observables do not seem to rapidly feed down and immediately drive unphysical behavior in lower order observables. In, for example, the order 28 observable results shown in Figs. 9–13 for 2D Euclidean Yang-Mills theory, the first appearance of unitarity bound violating Wilson loop expectations occurs at $\lambda \approx 1.3$, 1.65, and 1.9 for generator orders 2, 4 and 6, respectively. And yet nothing notable is visibly apparent at these coupling values in the displayed plots of smaller Wilson loop expectations. However, in the 2+1D Hamiltonian Yang-Mills theory results, the small oscillation spectrum is significantly more sensitive to higher order observables than low order observable expectation values and, for example, the visible bumps in the fourth order B_2^- and E^- curves of Fig. 17 are likely related to certain growing unphysical high order loop expectations which first exceed unity around $\lambda = 1.3$. Finally, in some cases as one moves to lower and lower values of gauge coupling, increasingly large (and unphysical) loop expectations can lead to genuine run away behavior and non-convergence of the ODE integration routine. This completely stops the progression to smaller values of coupling, and is the reason the generator order 6 results in 2+1D Yang-Mills shown in Fig. 15 do not extend below $\lambda = 1.4$; ODE convergence failed at $\lambda = 1.35$ after loop expectations exceeding one first appeared at $\lambda = 1.6$.

The final potential truncation-induced limitation mentioned above — namely, decent looking, internally consistent but increasingly inaccurate results — is seen to occur in calculations with order 2 generators and a single variational parameter. It is unsurprising that such calculations, once beyond the strong coupling regime, quickly become increasingly inaccurate despite not experiencing negative curvature modes or breakdown in ODE integration. With multiple variational parameters, one of the other issues above eventually always seems to occur.

In any infinite dimensional variational scheme, it is inevitable that understanding and minimizing truncation effects associated with the state representation is a major issue. As discussed in section V, this motivated the effort to explore a factorization-based approximation scheme for non-retained observables. This initial effort to implement an observable approximation scheme turns out to be rather disappointing. For any given observable truncation order, incorporating factorized approximations of non-retained observables using the implemented algorithm dramatically increases the number of terms in geodesic equations (and consequent storage requirements) but, as seen in Figs. 19 and 20, cannot be said to

lead to results which effectively mimic results from higher order but unapproximated observable truncations.

The basic idea motivating a factorization-based approximation scheme was that the typical electric flux sheet spanning a self-intersecting Wilson loop (in a confining theory) should truly look like the union of the typical flux sheets which would span each of the sub-loops produced by splitting the original loop at a self-intersection. The simple factorization $\langle W_\Gamma \rangle \approx \langle W_{\Gamma_1} \rangle \langle W_{\Gamma_2} \rangle$ for a self-intersecting loop $\Gamma = \Gamma_1 \Gamma_2$ should be a decent approximation if the flux sheets of the two sub-loops do not significantly interact, and if the sign of $\langle W_\Gamma \rangle$ agrees with the product of signs of the sub-loop expectations. But folded flux sheets do interact, as seen by the non-linear dependence on winding number in the logarithm of Wilson loop expectation values in one-plaquette models (or in other 2D Yang-Mills loop expectations [36]). Moreover, Wilson loop expectation values, while necessarily real, are not always positive. For these reasons, it was always clear that a simple factorization based approximation scheme will never be exact. The hope was that it could provide a good approximation for a sufficiently large fraction of observables to be an overall improvement. It should be the case that increasing lattice dimension increases the fraction of loops for which a simple factorization-based approximation works well, as increasing dimensions make it less likely that a generic loop will have a loop-spanning flux sheet with fold-induced flux interactions. So while the goal of developing a useful observable approximation scheme remains, more work is needed to explore possible schemes, especially on three dimensional lattices.

VII. CONCLUSION

It has always been clear that a numerical solution of large N Yang-Mills theory (or QCD) is a very tough computational task. The results presented in this paper on 2+1 dimensional Hamiltonian Yang-Mills theory illustrate what is currently practical using a desktop computer. The current software [30] is capable of performing analogous variational calculations in the lattice Hamiltonian formulation of 3+1 dimensional Yang-Mills theory, as well as calculations of the light meson spectrum in Hamiltonian formulations of 2+1 and 3+1 dimensional QCD. Initial results for these theories will be presented in a subsequent paper.

The 2+1 dimensional Yang-Mills results presented in section IV D may be viewed as a promising initial effort but are certainly more limited than one would like regarding how far it was feasible to push into the weak coupling regime.²⁵ Answering a variety of open questions will help determine the ultimate reach of this approach. On the purely computational side, it will be very helpful to understand:

1. Can the current *Gordion* program code be effectively implemented on a massively parallel high performance computing cluster? The challenge is whether inter-node

²⁵ However, it should be noted that there are no alternative methods, currently available, which can even begin to study non-Abelian Hamiltonian lattice gauge theories on infinite two or three dimensional lattices.

data transfer rates in a large cluster with a hierarchical memory architecture will be sufficient to enable efficient integration of the massive set of coupled geodesic equations when these equations are partitioned across a great many nodes.

2. Can GPUs be effectively utilized in the integration of the geodesic equations? This has not yet been explored. One aspect of this involves floating point precision. All work to date has used 64-bit floating point arithmetic in the integration of geodesic equations. If only 32-bit floating point arithmetic is used, will the resulting precision loss ever become problematic?

In terms of the achievable effectiveness of variational approximations, more conceptual open questions include:

3. Are there feasible alternatives to the strong-coupling order classification of observables which would provide superior selection criterion in a loop-list truncation? Euclidean lattice bootstrap efforts [13, 14] have used a simple cutoff on loop length to define selected subsets of Wilson loops. The strong-coupling order classification used in this work is more complicated to implement but, by design, produces superior results for a given truncation size in the strong coupling regime. Whether this remains true as one pushes into the weak coupling region, and whether some other selection criterion would be clearly superior, is unknown.
4. Similarly, is there a superior selection criterion for coherence group generators, other than simply using all generators up to a specified creation order (proportional to the number of plaquettes from which the generator is built)? The current code optionally implements a definition of generator normalization [30], which is a necessary first step for allowing meaningful comparisons of the relative importance of different generators as the minimization proceeds to smaller values of gauge coupling. But a detailed study of the relative importance of different generators is yet to be performed.
5. In Euclidean lattice simulations, much effort has been devoted to the development of improved lattice actions which speed up convergence to the continuum limit [37–39]. Analogous improved lattice Hamiltonians should be feasible to construct and implement in the coherent state approach. How much might this improve results?
6. Is it possible to formulate a more accurate, but practical, observable approximation scheme which performs better than the rather ad-hoc factorization algorithm described in section V? As clearly seen in tables II and III, the very rapid growth in the number of retained observables with increasing truncation order, and consequent growth in the amount of memory required to hold the geodesic equations, is a major limiting factor. Calculations to date have found that using order k generators with observables truncated at less than order $4k$ produce poor results. This is unsurprising as $4k$ is the minimal observable order for which all observable expectations appearing in curvature matrix elements (for the standard Kogut-Susskind Hamiltonian) are directly retained.

Is it possible to formulate an observable approximation scheme sufficiently accurate to allow good results to be obtained when using order k generators and observables truncated at less than order $4k$? Is it possible to identify, in a computationally efficient manner, those observables for which a factorization-based approximation is accurate, and only apply the approximation to such observables?

The 2+1D Yang-Mills theory results presented in section IV D show that limitations in the accuracy of the state representation — i.e., the loop-list truncation — are a critical issue restricting both how far any given calculation can be pushed into weak coupling, and how many variational parameters can be usefully included. Are there superior alternatives to a loop-list truncation? Specifically:

7. Will switching to a finite dimensional master field representation produce better results in the weak-coupling regime? In the old work [2], the Hamiltonian one-plaquette model was studied using both master field and loop-list state representations. As shown in Fig. 4 of that work, the master field results were found to exhibit curious non-monotonic behavior in the weak coupling regime, at couplings where the finite dimensional master field approximation could no longer well represent the tails of the increasingly compact eigenvalue distribution, leading to a view that loop-list state representations, despite their limitations, seemed more promising. On the other hand, a unitary finite dimensional master field approximation, despite being less accurate in the strong coupling regime (for comparable computational sizes), has the clearly desirable feature of never violating Wilson loop positivity constraints. Will master field truncation sizes achievable with modern computational resources allow one to reach weaker couplings than feasible with loop-list truncations in 2+1 and 3+1 dimensional Yang-Mills? This is clearly a key question to answer.
8. Are there fundamentally different choices for a coherence group, acting irreducible on the gauge invariant Hilbert space [1], which might allow completely different types of state representations? One possibility to explore could involve traces of products of equal-time Dirac propagators plus their time derivatives.

As noted in section III, the *Gordion* program code, along with extensive design and implementation notes, are freely available on Github [30]. Interested readers are encouraged to use this code base to explore some of the above questions. It is hoped that future work will shed light on their answers.

ACKNOWLEDGMENTS

Support from U.S. Department of Energy grant DE-SC0011637 is gratefully acknowledged.

[1] L. G. Yaffe, “Large N limits as classical mechanics,” *Rev. Mod. Phys.* **54**, 407 (1982).

[2] F. R. Brown and L. G. Yaffe, “The coherent state variational algorithm: A numerical method for solving large- N gauge theories,” *Nucl. Phys. B* **271**, 267–332 (1986).

[3] T. A. Dickens, U. J. Lindqwister, W. R. Somsky and L. G. Yaffe, “The coherent state variational algorithm. 2. Implementation and testing,” *Nucl. Phys. B* **309**, 1–119 (1988).

[4] E. Witten, “Baryons in the $1/N$ expansion,” *Nucl. Phys. B* **160**, 57–115 (1979).

[5] K. G. Wilson, “Confinement of quarks,” *Phys. Rev. D* **10**, 2445–2459 (1974).

[6] J. B. Kogut and L. Susskind, “Hamiltonian formulation of Wilson’s lattice gauge theories,” *Phys. Rev. D* **11**, 395–408 (1975)

[7] H. Meyer and M. Teper, “Confinement and the effective string theory in $SU(N \rightarrow \infty)$: a lattice study,” *JHEP* **12**, 031 (2004) arXiv:hep-lat/0411039 [hep-lat].

[8] M. Teper, “Large N ,” *PoS LATTICE2008*, 022 (2008), arXiv:0812.0085 [hep-lat].

[9] F. Bursa, R. Lau and M. Teper, “ $SO(2N)$ and $SU(N)$ gauge theories in 2+1 dimensions,” *JHEP* **05**, 025 (2013), arXiv:1208.4547 [hep-lat].

[10] A. Athenodorou, R. Lau and M. Teper, “On the weak N -dependence of $SO(N)$ and $SU(N)$ gauge theories in 2+1 dimensions,” *Phys. Lett. B* **749**, 448–453 (2015), arXiv:1504.08126 [hep-lat].

[11] A. Athenodorou and M. Teper, “ $SU(N)$ gauge theories in 2+1 dimensions: glueball spectra and k -string tensions,” *JHEP* **02**, 015 (2017), arXiv:1609.03873 [hep-lat].

[12] A. Athenodorou and M. Teper, “ $SU(N)$ gauge theories in 3+1 dimensions: glueball spectrum, string tensions and topology,” *JHEP* **12** (2021), 082, arXiv:2106.00364 [hep-lat].

[13] P. D. Anderson and M. Kruczenski, “Loop equations and bootstrap methods in the lattice,” *Nucl. Phys. B* **921**, 702–726 (2017), arXiv:1612.08140 [hep-th].

[14] V. Kazakov and Z. Zheng, “Bootstrap for lattice Yang-Mills theory,” *Phys. Rev. D* **107**, no.5, L051501 (2023) arXiv:2203.11360 [hep-th].

[15] Y. M. Makeenko and A. A. Migdal, “Exact equation for the loop average in multicolor QCD,” *Phys. Lett. B* **88**, 135 (1979) [erratum: *Phys. Lett. B* **89**, 437 (1980)].

[16] V. Kazakov and Z. Zheng, “Bootstrap for finite N lattice Yang-Mills theory,” *JHEP* **03**, 099 (2025), arXiv:2404.16925 [hep-th].

[17] Y. Guo, Z. Li, G. Yang and G. Zhu, “Bootstrapping $SU(3)$ lattice Yang-Mills theory,” *JHEP* **12**, 033 (2025), arXiv:2502.14421 [hep-th].

[18] H. W. Lin, “Bootstraps to strings: solving random matrix models with positivity,” *JHEP* **06**, 090 (2020), arXiv:2002.08387 [hep-th].

[19] R. d. Koch, A. Jevicki, X. Liu, K. Mathaba and J. P. Rodrigues, “Large N optimization for multi-matrix systems,” *JHEP* **01**, 168 (2022) arXiv:2108.08803 [hep-th].

[20] K. Mathaba, M. Mulokwe and J. P. Rodrigues, “Large N master field optimization: the quantum mechanics of two Yang-Mills coupled matrices,” *JHEP* **02**, 054 (2024), arXiv:2306.00935 [hep-th].

- [21] S. M. Dawid, Z. T. Draper, A. D. Hanlon, B. Hörz, C. Morningstar, F. Romero-López, S. R. Sharpe and S. Skinner, “QCD predictions for physical multimeson scattering amplitudes,” *Phys. Rev. Lett.* **135**, no.2, 021903 (2025), arXiv:2502.14348 [hep-lat].
- [22] S. M. Dawid, Z. T. Draper, A. D. Hanlon, B. Hörz, C. Morningstar, F. Romero-López, S. R. Sharpe and S. Skinner, “Two- and three-meson scattering amplitudes with physical quark masses from lattice QCD,” *Phys. Rev. D* **112**, no.1, 014505 (2025), arXiv:2502.17976 [hep-lat].
- [23] A. L. Fitzpatrick and E. Katz, “Snowmass white paper: Hamiltonian truncation,” arXiv:2201.11696 [hep-th].
- [24] E. Witten, “The $1/N$ expansion in atomic and particle physics,” *NATO Sci. Ser. B* **59**, 403-419 (1980)
- [25] S. R. Coleman, “ $1/N$,” SLAC-PUB-2484 (1980).
- [26] S. Coleman, “Aspects of Symmetry: selected Erice lectures,” Cambridge University Press, 1985, ISBN 978-0-521-31827-3.
- [27] U. J. Lindqwister, “Numerical studies of large N lattice gauge theories,” Princeton Univ. Ph.D. thesis, 1988, UMI-88-09316.
- [28] T. A. Dickens, “Numerical studies of fermionic field theories at large N ,” Princeton Univ. Ph.D. thesis, 1987 UMI-87-16885.
- [29] W. R. Somsky, “The coherent state variational algorithm and the QCD deconfinement phase transition,” Princeton Univ. Ph.D. thesis, 1989.
- [30] L. G. Yaffe, “Gordion: Design and Implementation,” Github repository.
- [31] D. J. Gross and E. Witten, “Possible third order phase transition in the large N lattice gauge theory,” *Phys. Rev. D* **21**, 446–453 (1980).
- [32] S. R. Wadia, “ $N = \infty$ phase transition in a class of exactly soluble model lattice gauge theories,” *Phys. Lett. B* **93**, 403–410 (1980).
- [33] A. Jevicki and B. Sakita, “Loop space representation and the large N behavior of the one plaquette Kogut-Susskind Hamiltonian,” *Phys. Rev. D* **22**, 467 (1980).
- [34] H. Neuberger, “Nonperturbative contributions in models with a nonanalytic behavior at infinite N ,” *Nucl. Phys. B* **179**, 253-282 (1981).
- [35] D. Friedan, “Some Nonabelian toy models in the large N limit,” *Commun. Math. Phys.* **78**, 353 (1981).
- [36] V. A. Kazakov, “Wilson loop average for an arbitrary contour in two-dimensional $U(N)$ gauge theory,” *Nucl. Phys. B* **179**, 283-293 (1981).
- [37] K. Symanzik, “Continuum limit and improved action in lattice theories. 1. Principles and φ^4 theory,” *Nucl. Phys. B* **226**, 187-204 (1983).
- [38] P. Weisz, “Continuum limit improved lattice action for pure Yang-Mills theory. 1.,” *Nucl. Phys. B* **212**, 1-17 (1983).
- [39] P. Weisz and R. Wohlert, “Continuum limit improved lattice action for pure Yang-Mills theory. 2.,” *Nucl. Phys. B* **236**, 397 (1984) [erratum: *Nucl. Phys. B* **247**, 544 (1984)].